Clarkson University

THERMOELECTRIC POWER GENERATION SYSTEM OPTIMIZATION STUDIES

a dissertation

by

Madhav A Karri

department of Mechanical and Aeronautical Engineering

Wallace H. Coulter School of Engineering

Clarkson University

Potsdam, NY 13699 - 5725

Submitted in partial fulfillment of the requirements

for the degree of

Doctor of Philosophy

in

Mechanical Engineering

January 2011

Accepted by the Graduate School

Date

Dean

The undersigned have examined the dissertation entitled

Thermoelectric Power Generation System Optimization Studies

presented by Madhav A. Karri, a candidate for the degree of Doctor of Philosophy (Mechanical Engineering), and hereby certify that it is worthy of acceptance.

Date

ADVISOR Dr. Brian T. Helenbrook

EXAMINING COMMITTEE

Dr. Eric F. Thacher

Dr. Frederick M. Carlson

Dr. Kenneth D. Willmert

Dr. Kathleen Fowler

Abstract

A significant amount of energy we consume each year is rejected as waste heat to the ambient. Conservative estimates place the quantity of energy wasted at about 70%. Converting the waste heat into electrical power would be convenient and effective for a number of primary and secondary applications. A viable solution for converting waste heat into electrical energy is to use thermoelectric power conversion. Thermoelectric power generation is based on solid state technology with no moving parts and works on the principle of Seebeck effect. In this work a thermoelectric generator (TEG) system simulator was developed to perform various parametric and system optimization studies. Optimization studies were performed to determine the effect of system size, exhaust and coolant flow conditions, and thermoelectric material on the net gains produced by the TEG system and on the optimum TEG system design. A sports utility vehicle was used as a case study for the application of TEG in mobile systems.

Nomenclature

Symbol	Units	Description
Upper Case Roman		
A	m^2	Heat transfer area, $(A_f + A_b)$.
A_b	m^2	Prime surface area.
A_c	m^2	Flow cross-sectional area.
A_e	m^2	Heat transfer area, exhaust side.
A_f	m^2	Heat transfer area, coolant side.
		Fin surface area.
A_l	m^2	Cross sectional area of thermoelectric leg.
A_{xy}	m^2	TEG system size or plan area.
$F(\overrightarrow{x})$	$-$	Function that needs to be solved.
Ⓗ	$-$	Constant heat rate per unit tube length.
I	$amps$	Current or total current of the generator.
$J(\overrightarrow{x})$	$-$	Jacobian of $F(\overrightarrow{x})$.
L	m	Flow length of uninterrupted fin.
L_x	m	Length of TEG parallel to exhaust or
		coolant flow streams.

L_y	m	Length of TEG normal to exhaust or coolant flow streams.
K	$\frac{W}{K}$	Thermal conductance.
K_g	$\frac{W}{K}$	Device thermal conductance.
N_c	$-$	Total number of couples.
N_m	$-$	Total number of thermal sections or modules in a TEG.
Nu	$-$	Nusselt number.
P	W	Power.
P_g	W	Total electrical power from the generator.
P_L	W	Total parasitic losses.
P_{net}	W	Net power.
P_P	W	Coolant pumping power.
Pr	$-$	Prandtl number.
Q	$\frac{m^3}{s}$	Volumetric flow rate.
Q_T	$\frac{m^3}{s}$	TEG volumetric flow rate.
R	Ω	Resistance.
R_g	Ω	Device electrical resistance.
R_L	Ω	Load resistance.
R_i	Ω	Internal resistance of a couple of module.
Re	$-$	Reynolds number.
T_c	K	Cold junction temperature.
T_e	K	Bulk temperature of exhaust.
$\overline{T}_e$	K	Average bulk temperature of exhaust.
$T_{e,i}$	K	Exhaust inlet temperature.
T_f	K	Bulk temperature of coolant.

$\overline{T}_f$	K	Average bulk temperature of exhaust.
$T_{f,i}$	K	Coolant inlet temperature.
T_h	K	Hot junction temperature.
$T_{h,max}$	K	Maximum allowable hot junction temperature.
T_m	K	Mean temperature.
T_w	K	Wall temperature.
Ⓣ	–	Constant wall temperature.
$\overline{U}$	$\frac{W}{m^2K}$	Average overall heat transfer coefficient.
$\overline{U}_e$	$\frac{W}{m^2K}$	Average overall heat transfer coefficient, exhaust side.
$\overline{U}_f$	$\frac{W}{m^2K}$	Average overall heat transfer coefficient, coolant side.
V	$volts$	Voltage or total voltage of the generator.
V_{oc}	$volts$	Open circuit voltage.
W_T	kg	Weight of TEG system.
Z	$\frac{1}{K}$	Couple or device thermoelectric figure of merit.

Lower Case Roman

b	m	Plate spacing of heat exchanger.
c_{p_e}	$\frac{J}{kgK}$	Specific heat of exhaust.
c_{p_f}	$\frac{J}{kgK}$	Specific heat of coolant.
f	–	Friction factor.
h	$\frac{W}{m^2K}$	Heat transfer coefficient.
j	–	Index counter.
	–	Colburn factor.
k	$\frac{W}{mK}$	Thermal conductivity.
	$\frac{1}{m^4}$	Loss coefficient.
$\overline{k}$	$\frac{W}{mK}$	Thermal conductivity of a thermoelectric material averaged over T_h and T_c.

k_E	$\frac{1}{m^4}$	Loss coefficient of engine.
k_e	$\frac{1}{m^4}$	Lumped exhaust loss coefficient.
	$\frac{W}{mK}$	Thermal conductivity of exhaust.
k_f	$\frac{W}{mK}$	Thermal conductivity of coolant.
k_S	$\frac{1}{m^4}$	Equivalent system loss coefficient.
k_T	$\frac{1}{m^4}$	Loss coefficient of TEG circuit.
$\overline{k}_n$	$\frac{W}{mK}$	Thermal conductivity of a n-type thermoelectric material averaged over T_h and T_c.
$\overline{k}_p$	$\frac{W}{mK}$	Thermal conductivity of a p-type thermoelectric material averaged over T_h and T_c.
l_l	m	Length of thermoelectric leg.
m	$-$	Ratio of load resistance to internal resistance.
$\dot{m}$	$\frac{Kg}{s}$	Mass flow rate.
$\dot{m}_e$	$\frac{Kg}{s}$	Mass flow rate of the exhaust.
$\dot{m}_f$	$\frac{Kg}{s}$	Mass flow rate of the coolant.
n_x	$-$	Number of zones parallel to L_x.
n_y	$-$	Number of cells in a single n_x zone.
q_h	W	Heat input into the thermoelectric couple or module.
r_h	m	Hydraulic radius.
s	m	Fin spacing.
$\overline{x}$	$-$	Property of a thermoelectric material averaged over T_h and T_c.
$\vec{x}$	$-$	Vector of unknowns.
z	$\frac{1}{K}$	Material thermoelectric figure of merit.

Upper Case Greek

ΔP_B	W	Parasitic blow-down power.
ΔP_D	W	Parasitic power to transport TEG system weight.
ΔP_P	W	Parasitic coolant pumping power.
Δp	Pa	Pressure drop.
Δp_P	Pa	Pump pressure rise.
Δp_T	Pa	Pressure rise available to TEG circuit.
ΔT	K	Temperature difference.
ΔT_g	K	Device average junction temperature difference.

Lower Case Greek

α	$-$	Aspect ratio of rectangular channel.
α	$\frac{V}{K}$	Seebeck coefficient.
α_g	$\frac{V}{K}$	Device Seebeck coefficient.
$\overline{\alpha}_n$	$\frac{V}{K}$	Seebeck coefficient of a n-type thermoelectric material averaged over T_h and T_c.
$\overline{\alpha}_p$	$\frac{V}{K}$	Seebeck coefficient of a p-type thermoelectric material averaged over T_h and T_c.
β	$\frac{1}{m}$	Heat transfer area per unit volume between heat exchanger plates.
γ	$\frac{1}{m}$	Aspect ratio of thermoelectric leg.
δ	m	Fin thickness.
ζ	$\frac{1}{m^2}$	Couple density.
η_{aa}	$-$	Alternator or AC generator efficiency.
η_D	$-$	Driveline transmission efficiency.
η_g	$-$	Thermal efficiency of a thermoelectric couple, module or generator.

η_P	$-$	Coolant pump efficiency.
η_{pcu}	$-$	PCU efficiency.
μ_D	$-$	Rolling resistance coefficient.
μ_e	$\frac{Pa}{s}$	Dynamic viscosity of exhaust.
μ_f	$\frac{Pa}{s}$	Dynamic viscosity of coolant.
ν	$\frac{m^2}{s}$	Kinematic viscosity.
ρ	Ωm	Electrical resistivity or density.
ρ_e	$\frac{kg}{m^3}$	Density of exhaust gas.
ρ_f	$\frac{kg}{m^3}$	Density of coolant.
$\overline{\rho}$	Ωm	Electrical resistivity of a thermoelectric material averaged over T_h and T_c.
$\overline{\rho}_n$	Ωm	Electrical resistivity of a n-type thermoelectric material averaged over T_h and T_c.
$\overline{\rho}_p$	Ωm	Electrical resistivity of a p-type thermoelectric material averaged over T_h and T_c.
τ	$-$	Unit surface shear stress.
υ	$\frac{m}{s}$	Velocity of vehicle.

Acronyms

0	$-$	Baseline case (no TEG).
AC	$-$	Alternating current.
AETEG	$-$	Automobile exhaust thermoelectric generator.
CHX	$-$	Coolant heat exchanger.
CNG	$-$	Compressed natural gas.
$ceq\left(\vec{x}\right)$	$-$	Set of equality constraints.
$c\left(\vec{x}\right)$	$-$	Set of inequality constraints.

emf	–	Electro motive force.
EHX	–	Exhaust heat exchanger.
FP	$\frac{1}{m}$	Fin pitch.
GMC	–	General Motors Corporation.
Hi-Z	–	Hi-Z Technology Inc.
lb	–	Lower bound on design variables.
NREL	–	National Renewable Energy Laboratory.
PCU	–	Power conditioning unit.
TEG	–	Thermoelectric generator.
TEPG	–	Thermoelectric power generator.
TPG	–	Thermoelectric power generation.
ub	–	Upper bound on design variables.

Contents

List of Figures

List of Tables

Chapter 1

Introduction

Each year the society spends a tremendous amount of its energy resources and a significant fraction of this energy resources consists of fossil fuels which were created several hundred million years ago and are non-renewable. Conservative estimates place the quantity of energy wasted at about 70%. An estimate of the U.S. energy consumption and rejection through various streams is shown in figure (1.1). The flow chart shows that a significant amount of energy is being rejected to the ambient in the electricity generation and the transportation sectors. This is due to the inefficient utilization of energy resources and system inefficiencies. A possible solution to the dwindling energy resources would be to minimize the waste through improved system efficiencies and efficient utilization of energy resources.

As shown in figure (1.1), a predominant fraction of the global energy resources are being converted into thermal energy and after utilization the remainder is rejected as waste heat to the ambient. Some common characteristics of the waste heat sources are listed below [1]:

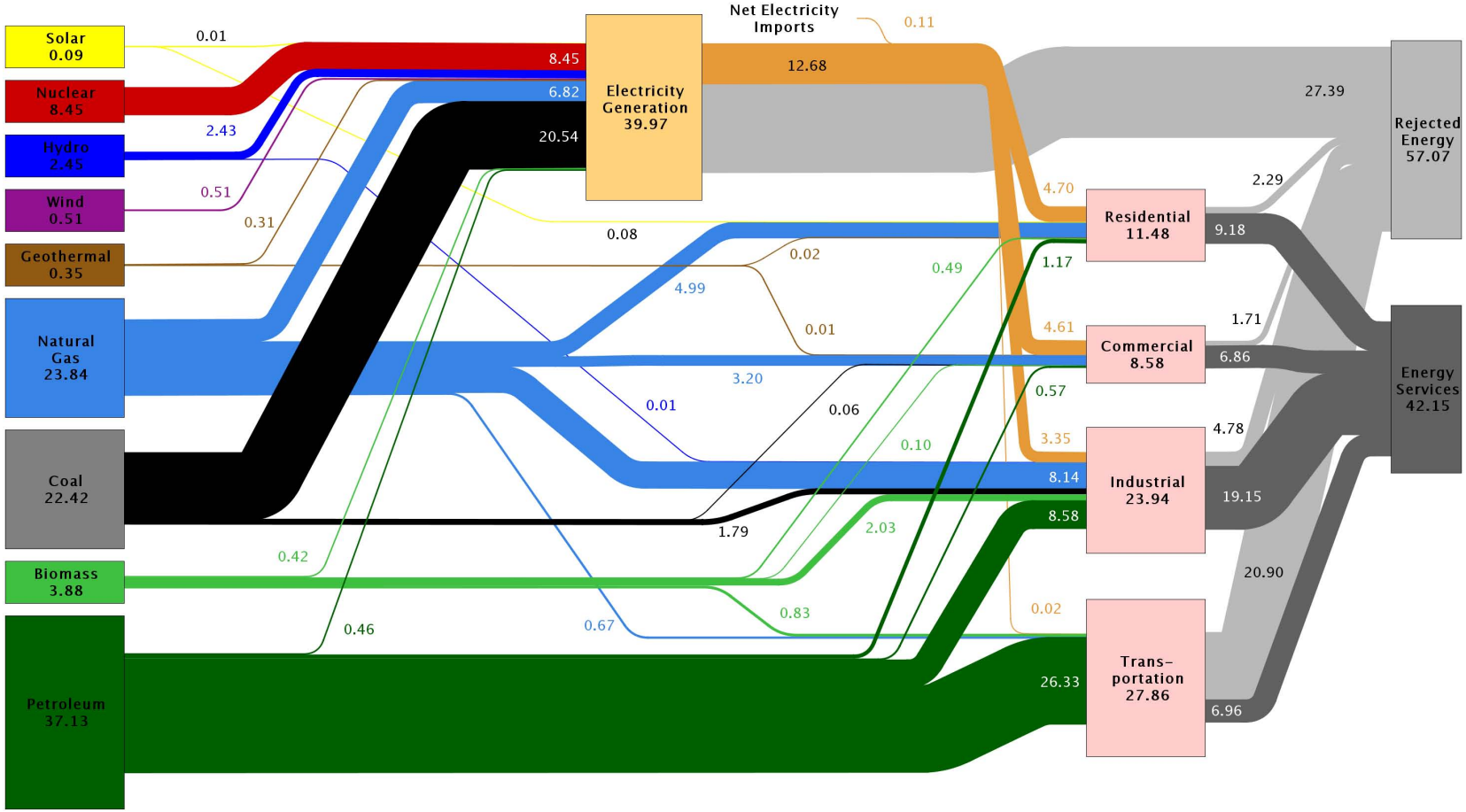

Figure 1.1: Estimated U.S. energy consumption in 2008: 99.2 Quads (Credit and data source: Lawrence Livermore National Laboratory and U.S. Department of Energy).

- Large number of small-scale and dispersed energy sources.
- Wide range of temperature.
- Unsteady variation of heat sources in terms of mass flow rate and temperature.
- Various states of heat carriers, such as chemically reactive gas, solid material, and liquid medium.
- Difficulty of handling.
- Low energy density per volume or per weight.

Waste heat can be reutilized as a heat source for other processes. However, often it is difficult to match efficient reutilization processes to sources. In contrast, converting the waste heat into electrical power would be convenient and effective for a number of primary and secondary applications. Generating electricity using conventional energy conversion would necessitate the need for a stable and high energy density source which is unlike the characteristics of a waste heat source. However, a viable solution for converting waste heat into electrical energy is to use thermoelectric power conversion. Thermoelectric power generation (TPG) is based on solid state technology with no moving parts and can be easily adapted to wide range of operating conditions.

1.1 Motivation

Systems based on petroleum account for a significant fraction of the waste heat utilization sector and fuels based on petroleum have assumed a position of leadership in the transportation and energy sector (about 37% from figure (1.1)). However, due to factors such as our dependence on depleting oil reserves and environmental issues, alternative fuels and propulsion systems are being sought that can provide an increase in efficiency and reduction in emissions.

Engine description	Engine loading (%) max power	Combustion energy (%)		
		shaft	exhaust	coolant and ambient
1991 Dodge Caravan 3.0L (102kW) SI Engine	30	26.3	27.2	46.5
	60	18.1	24.6	57.3
	90	17.5	24.7	57.8
Caterpillar 3126E 7.2L (205kW) Diesel Engine	30	38.5	22.0	39.5
	60	38.0	22.7	39.3
	90	40.5	20.0	39.5
DDC Series 60 12.7L (330kW) Diesel Engine	30	41.0	25.2	33.8
	60	43.3	24.3	32.4
	90	44.0	22.0	34.0
John Deere 8.1L (186kW) CNG SI Engine	30	37.8	23.7	38.5
	60	37.4	21.4	41.2
	90	37.9	19.4	42.7

Table 1.1: Energy budget for various gasoline, diesel, and natural gas engines at different engine loadings

The energy budget for various gasoline, diesel, and natural gas engines at engine loadings of 30, 60, and 90% of their maximum rated power is tabulated in table 1.1. The listed engines are employed for various stationary and mobile applications. The data was based on the engine maps from the fuel converter library in "ADVISOR", a vehicle system analysis tool [2]. From the results shown in table 1.1, approximately 20 to 30% of the available energy in the fuel converter is rejected as heat to the exhaust and 30 to 55% to the coolant and ambient through conduction, convection, and radiation. As a result only 15 to 45% of the original energy contained in the fuel is converted into shaft power of the engine. Depending on the application, a limited or complete portion of the shaft power is converted into electrical power. Therefore a means to improve the fuel economy is to increase the overall efficiency of the powertrain by recovering waste heat from the exhaust and converting it into electrical energy. A thermoelectric generator (TEG) system can be used to convert this heat energy into electrical power.

The TEG works on the principle of the Seebeck effect, when the junctions formed by joining two dissimilar current carrying conductors are maintained at different temperatures, an electro motive force (emf) is generated in the circuit. The current carrying conductors are known as thermoelectric elements and the couple formed out of the two current carrying conductors is known as a thermoelectric couple. In a typical generator, heat exchangers are used to transfer heat from the heat source and to the heat sink through the junctions of the thermocouple. The heat exchangers and the thermoelectric couple unit is known as a TEG. A TEG based on the above description is shown in figure (1.2). The two dissimilar current carrying conductors

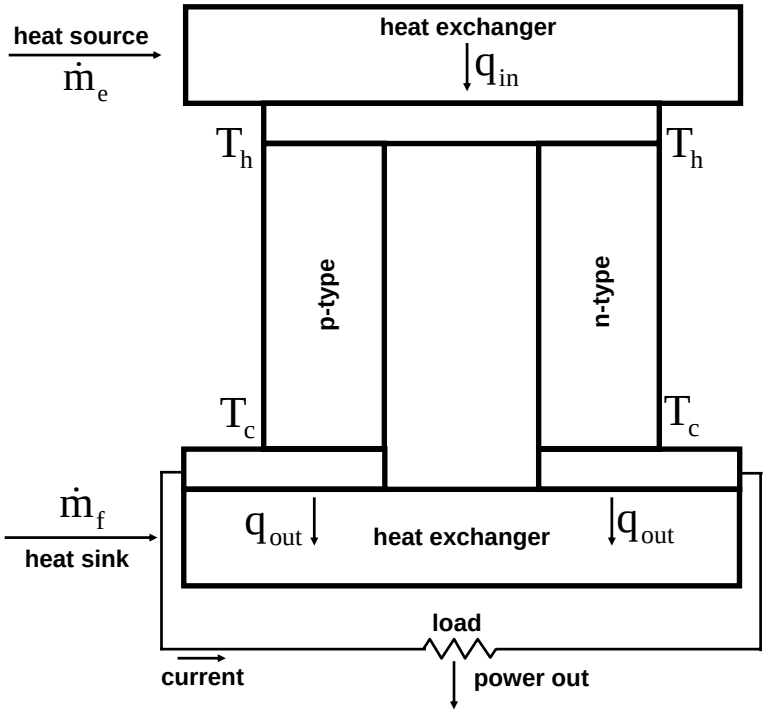

Figure 1.2: A typical TEG

are formed out of n and p-type semiconductor materials and referred to as n and p-type thermoelectric materials.

1.2 Background

A large number of theoretical and experimental studies have been performed to evaluate the feasibility of systems converting waste heat into electrical power using thermoelectric energy conversion. An extensive study and a review of experimental investigation of systems converting industrial waste heat to electrical power using thermoelectric energy conversion was carried out by Takenobu Kajikawa [1] of Shonan Institute of Technology. Kajikawa studied various sources of industrial waste heat and their characteristics. The experimental investigations reported in his studies are listed below:

- Wall-embedded-type system: TEG systems were installed in the upper region of a furnace and at the exhaust gas duct near the stack in a small-scale fluidized bed-type incinerator. The hot junction surface of the test unit was covered with 18 mm thick SiC cement layer to protect it against chemically reactive exhaust gas. The test unit was positioned such that the open face of the SiC cement layer was in alignment with the other refractory walls. The generator consisted of 4 Pb-Te-Sn modules, each capable of generating 125 $watts$ of electrical power. The bulk temperature of the gas varied between 1073 and 1223 K and the hot junction surface temperature of the test unit varied between 993 and 843 K. The hot junction temperature at the module was estimated to be about 785 K. The total power generated by the TEG system was about 135.9 $watts$ compared to the design power of 550 $watts$. Discrepancy between the design and the experiment was due to the inaccurate estimation of the heat resistance at the wall surface covered by SiC cement and the contact heat resistance between the SiC cement and hot junction surface of the thermoelectric unit. In addition due to the low gas velocity, heat transfer was achieved only through radiation.

- In-line-type system in a batch-type incinerator: a 1 kW class in-line-type TEG system was tested in a batch-type incinerator processing 200 kg of municipal solid waste per day. The temperature of the exhaust gas was about 1473 K. However, due to the upper operating temperature limit of the thermoelectric module the exhaust gas temperature was reduced to 523 K by diluting it with air. The total power output from the generator was about 1177.5 $watts$. Thermoelectric modules with higher operating temperature limits could produce more power resulting in an increase in generator efficiency.

- In-line-type system in internal-combustion power plant: on-site experiment to study the feasibility of using an in-line type TEG system to recover waste heat from the exhaust of a 100 MW internal combustion power plant was carried out. The exhaust gas temperature was about 643 to 453 K. The TEG system consisted of 16 thermoelectric modules and each module consisted of 80 couples made from Bi_2Te_3 thermoelectric material. The total power output from the generator was about 526 $watts$.

- Air heat-exchange-type system: field testing of a TEG system installed inside a hot air duct was performed. The hot air duct was a preheated air feeding duct to the burner of an incinerator. The incinerator had a processing rate of 40 $tons$ of municipal solid waste per day and the operating time was 16 hours per day. The TEG system consisted of 84 Bi_2Te_3 modules. The exhaust gas inlet temperature was 523 K and the outlet temperature was 503 K. Water was used as the heat sink fluid with an inlet temperature of 296 K. The total power output from the generator was about 230 $watts$.

- Organic medium heat-exchange-type system: contrary to the conventional means of transferring waste heat directly to a TEG system, heat from an incinerator, processing 500 *tons* of municipal solid waste per day, was transferred initially to an organic medium through a heat exchanger and later from the organic medium to the TEG system. Such a system would result in a stable power output irrespective of the fluctuations in the waste heat characteristics such as temperature and flow rate. Liquid such as diphenyl or diphenyl ether was used as the organic medium. Heat transfer from the gas to the liquid medium was accomplished using either a shell and tube-type or shell and plate-type heat exchanger. The TEG system had a total of 11 stacks of heat exchanging copper plates, 5 were used as the heat sources and the remaining 6 were used as the heat sinks. The complete system had a total of 60 thermoelectric modules and each module consisted of 50 thermoelectric couples. Conventional Bi_2Te_3 thermoelectric material was used in these modules. The total power output from the system was 535.8 *watts* at a heat source fluid temperature of 537 K and flow rate of 37.5 $\frac{L}{min}$.

- Heat pipe-type system: testing of a TEG system using heat pipe as the heat source was carried out. One end of the heat pipe was located across the exhaust gas flow while the other end formed an integral part of the TEG system. Each TEG system consisted of a heat pipe unit, 3 thermoelectric modules, and a heat sink unit. Each thermoelectric module consisted of 49 couples of Bi_2Te_3 thermoelectric material. A total of 24 such TEG systems were installed in the exhaust gas duct. The exhaust gas inlet temperature was 513 K and the gas velocity was 18 $\frac{m}{s}$. Water was used as the heat sink fluid with an inlet temperature of 298 K and the flow rate was 30 $\frac{L}{s}$. The design power from the complete system was 600 *watts* and the maximum power output attained by the system was about 570 *watts*.

Based on the above experimental studies, Kajikawa related the feasibility of TEG systems to 2 important aspects:

- enhancement of system efficiency and
- enhancement of system reliability in both the energy source and thermoelectric module.

Improving the system efficiency is governed by two important factors, enhancement of heat transfer phenomena particularly at the heat source and secondly, the availability of better thermoelectric materials. Even with the present-day thermoelectric bulk materials a significant improvement in the system efficiency can be achieved just by enhancing the heat transfer phenomena. An enhancement in the heat transfer phenomena while maintaining a low pressure drop can be achieved by making use of designs and technologies such as heat transfer surface with wing-shaped pin-fins and advanced heat pipe systems. In addition the electrical power output and the conversion efficiency can be further improved by reducing the thermal and electrical contact resistances. Reducing the thermal contact resistance has a more significant effect on increasing the power output than reducing the electrical contact resistance particularly for a low-temperature waste heat application. However, reduction of thermal resistance between the heat transfer surface and the thermoelectric module is in general contrary to the enhancement of reliability. Tests were conducted to evaluate system reliability as a function of consistent performance of the thermoelectric modules. During these tests electrical resistance of the modules increased by 5 to 27%, 5 to 14% increase was registered at a continuous operating time of 300 hours and 15 to 27% increase was registered at a continuous operating time of 7600 hours.

Kajikawa summarized the results from his experimental studies as follows:

- The power generated by the TEG systems met the design specifications except for the wall-embedded-type.
- Conventional Bi_2Te_3 thermoelectric material was used in all of the experimental studies except for the wall-embedded type in which *Pb-Te-Sn* thermoelectric material was used. The temperature regime for the wall-embedded type was about 800 K and the *Pb-Te-Sn* has better performance characteristics at this temperature regime in comparison to the Bi_2Te_3 material.
- The energy conversion efficiency for the above experimental studies varied between 2.4 and 3.6%.

As discussed earlier, systems based on petroleum, specifically in the transportation sector, also account for a significant fraction of the waste heat utilization sector. Therefore a substantial amount of design, theory and experimental investigations on converting waste heat into electricity using thermoelectric energy conversion in such systems have also been carried out. Some of these investigations are discussed below.

One of the early studies on a TEG was performed by Richard H. Bauer of Clarkson University during 1961-1963 [3]. Bauer investigated the feasibility of designing a TEG which could provide auxiliary electrical energy for an automobile. The engine cooling water was used as the heat source while the cold junction heat exchanger used ambient air as the heat sink. Lead telluride was the only thermoelectric material considered for this study. The investigation showed that a TEG using the engine cooling water as a heat source would not be feasible, due to the large volume and cross-sectional area of thermoelectric material necessary to yield the required electrical power output. The large volumes and cross-sectional areas required are attributed to the combined effects of the low Carnot and low thermocouple efficiencies encountered by operating

with the relatively low-grade heat source. It was also concluded that utilizing a thermoelectric generator on an automotive engine was worthy of further investigation if the heat source could be kept close to 600 K.

Parallel to Bauer's work, Anthony Joseph Tomarchio of Clarkson University conducted a feasibility study of increasing an automobile engine efficiency by replacing the alternator with a TEG by converting waste energy in the exhaust gases to electrical power [4]. Air was used as the heat sink fluid and lead telluride as the thermoelectric material. The principal conclusions from this study were as follows: (1) the maximum power requirements of 514 *watts* at 14.7 *volts* could be met at approximately 50 (mph), (2) the combined power output of the battery and the generator below 50 (mph) down to 20 (mph) would provide the minimum power requirements, and (3) unless improved semiconductors materials become available, the minimum power requirements cannot be satisfied at speeds below 20 (mph).

Birkholz et al. designed a TEG that uses $FeSi_2$-thermoelements [5]. They tested their generator on a Porsche 944 engine and reported a maximum electrical power of 58 *watts* at full engine power. A total of 90 thermoelements were used in the generator.

A significant work in the design, construction and testing of a TEG for mobile applications was performed by Hi-Z Inc. Bass et al. at Hi-Z studied novel methods of recovering waste heat from Diesel engines [6]. The study consisted of evaluating various heat sources: energy lost through the radiator, the intercooler, the lubricating oil system, and the exhaust in diesel engines. They concluded that the exhaust system offered the most potential for thermoelectric based heat recovery due to the high available temperature difference between the heat source and the heat sink. In the same study Hi-Z also investigated various thermoelectric materials compatible with these heat sources to determine the materials and generator configuration required

to achieve the most economic and direct conversion of heat to electricity. The thermoelectric materials that were studied consisted of Bi_2Te_3, lead-telluride, and silicon-germanium family of alloys. Their study concluded that the Bi_2Te_3 offered the best performance in spite of its lower maximum operating temperature. Use of Bi_2Te_3 system minimizes the amount of heat transfer area required to conduct the heat into the thermoelectric elements. This decreases the pressure drop across the exhaust heat exchanger resulting in a lower back pressure on the engine. Based on these studies, using exhaust gas and Bi_2Te_3 as the heat source and the thermoelectric material, Hi-Z designed and tested a 1 kW prototype TEG [7]. The prototype thermoelectric generator consisted of seventy two 13 *watt* Bi_2Te_3 thermoelectric modules. The prototype TEG was tested on a 14 L 350 hp Cummins NTC engine. A maximum power output of 1068 Watts was obtained at 300 hp and 1700 rpm.

Ikoma et al. at Nissan Research Center, designed a TEG using silicon germanium ($SiGe$) thermoelectric modules [8]. The module consisted of eight couples of p-type and n-type $SiGe$ elements. The maximum electrical power output from the module is approximately 1.2 $watts$. A total of 72 such modules were used in the generator. The modules were arranged between an exhaust pipe with a rectangular cross section and water jackets around the exhaust pipe. The generator was installed in a 3000 $c.c$ engine vehicle. A maximum electrical power output of 35.6 $watts$ was produced by the generator at 60 $\frac{km}{h}$ during an uphill climb.

Crane et al. did a theoretical study to evaluate the integration of thermoelectric modules into the radiator system of an automobile [9]. The study was performed under the assumption that 30 to 50% of the total fuel energy may be expelled through the radiator. The objective of their study was to design a thermoelectric radiator system, that can displace the alternator system. Bi_2Te_3 thermoelectric material was used in their studies. The modeling was performed based on the dimensions of typical stock radiator used in GM Chevrolet Suburban. After validating the baseline radiator model (without the thermoelectric modules) against actual radiator performance data, studies were performed to find the optimal modifications to the radiator dimensions that would achieve high thermoelectric power output with minimal additional system weight and parasitic losses. The study concluded that: (1) with current (Bi_2Te_3) thermoelectric technology it might be feasible to displace current day alternator system with such a thermoelectric radiator and (2) penalties such as increased radiator size or increased accessory power are minimal.

Vazequez et al. [10] reviewed "the main characteristics and evolution of the different investigations performed over the last three decades concerning the use of TPG using the heat from the exhaust gases produced in the combustion process of an automobile." Their study concluded that the maximum electrical power generated in TEGs for cars has varied between 43 to 193 $watts$. This power was achieved normally in a car running at 65 $\frac{km}{h}$ uphill. However, the same TEGs have been inefficient for other working conditions, such as during idling, because the temperature range of the exhaust gas did not match with the optimal working temperatures of the thermoelectric modules.

From the above reviewed literature, it can be noticed that none of the studies conducted in the past reported any precise estimates of fuel savings, which is the final objective of a TEG being installed in an automobile, or the effects of the TEG on vehicle systems. Therefore to address these missing details Thacher et al. [11] tested a prototype automobile exhaust thermoelectric generator (AETEG) installed in a 1999 General Motors Corporation (GMC) Sierra pick-up truck. Testing was performed in a dynamometer-equipped wind tunnel at Delphi Corporations Harrison Thermal Systems Division in Lockport, New York. Some of the important outcomes of the tests were, exhaust pipe insulation upstream of the TEG and lowering the coolant temperature had a significant positive effect on the power, parasitic losses resulting from the AETEG weight and the coolant pumping power were significant but manageable, and the increased exhaust flow resistance and the additional heat load from the AETEG were not significant effects.

As shown by the literature reviewed, an extensive number of experiments have been performed and models have been developed to evaluate the performance and feasibility of thermoelectric power conversion based on waste heat utilization. Based on the work and results from these experiments and models, the following observations are made:

- a majority of these experiments have focussed on evaluating the power producing capabilities of the TEG, using bulk thermoelectric materials, under a given heat source characteristics,
- the TEGs in these experiments were not operating to their maximum potential, as a result the energy available from the heat source was underutilized,
- the design of these generators was neither optimized to maximize the power or the performance,

- a majority of these experiments and models have not accounted for the parasitic losses occurring due to the interface of the TEG with the heat source and the heat sink, and
- some of the designs [12] have been optimized, accounting for various parasitic losses. However, these designs were either system specific or the optimization was not based on the overall system perspective.

Therefore a generic optimization tool that maximizes the gains produced by the TEG system is needed. One such tool has been developed by Terry J. Hendricks and Jason A. Lustbader at National Renewable Energy Laboratory (NREL) [13, 14]. Christened as advanced thermoelectric power system investigations for light duty and heavy duty applications, the tool has the following features [13]:

- simultaneously analyzes the interdependent effect of heat exchanger performance and thermoelectric device performance,
- simultaneously optimizes the heat exchanger/thermolectric power generator (TEPG) system to obtain the highest TEPG system efficiency and power output in any vehicle waste heat recovery application,
- can analyze segmented-thermoelectric-material designs and single-thermoelectric-material designs, quantum-well designs, and thin-film super-lattice designs,
- outputs the optimum design parameters as a function of TEPG hot side and cold side temperatures, and
- has been integrated with NRELs ADVISOR to provide TEPG/heat exchanger optimum design parameters for any vehicle configuration and drive cycle.

However, based on the results reported in [13] and [14], instead of generating an optimal design specification the tool generates an optimal design space. This was due to the analysis being based on the parametric study approach rather than using an optimization search criteria. The tool did not account for any parasitic losses, as was the case in the majority of the experimental and modeling studies. As a result the selection of optimal design space was based on the objective to maximize the power from the TEG. An ideal analysis tool should try to maximize either the net gain in power generated by the TEG system or the gains in fuel savings. Therefore a major objective in this work was to develop a generic optimization tool that maximizes the overall system efficiency.

1.3 Outline

This dissertation is organized as follows: the subsequent chapter gives a description and model of the TEG system and simulator. This is followed by a TPG optimization problem statement and a system description of two case studies, a sports utility vehicle (mobile application) and a compressed natural gas (CNG) engine (stationary application) was performed. Subsequently, a state space analysis was performed to investigate for any interdependencies between various design variables. Based on the results from the state space analysis, the optimization problem is redefined and the optimization results from the two case studies are discussed. In the last chapter conclusions from this work are summarized and the future course of work is discussed.

Chapter 2

TEG System and Simulator

As stated previously, the simulator constitutes an important component of the TEG optimization. Thus, the focus of this chapter is exclusively on the description and modeling of the TEG. As discussed earlier, the TEG works on the principle of the Seebeck effect: when the junctions formed by joining two dissimilar current carrying conductors are maintained at different temperatures, an electro motive force (emf) is generated in the circuit. The current carrying conductors are formed out of p-type and n-type thermoelectric materials and the couple formed out of the two current carrying conductors is known as a thermoelectric couple. In a typical TEG, heat exchangers are used to transfer heat from the heat source and to the heat sink through the junctions of the thermocouple.

The performance of the TEG is a function of the thermoelectric material properties, heat source and sink's mass flow rate, inlet temperature, and fluid properties, and finally the heat exhangers design. The performance of the thermoelectric materials is determined by three thermoelectric properties: Seebeck coefficient, electrical resistivity, and thermal conductivity. Therefore, this chapter starts with an analysis that correlates the performance of the TEG to the thermoelectric properties. For practical applications and feasibility in the construction of the TEG, a number of thermoelectric couples are put together to form a thermoelectric module. Therefore in the subsequent section a description and the elements of the thermoelectric module are described. This is followed by a description and modeling of a generic TEG simulator. This includes a description of the thermoelectric materials properties, heat exchangers type and performance, and heat source and heat sink fluid properties.

2.1 TEG: Efficiency and Figure of Merit

Figure (2.1) illustrates a thermoelectric circuit (or couple) consisting of two dissimilar homogeneous materials A and B, their junctions maintained at hot junction temperature T_h and cold junction temperature T_c ($T_h > T_c$), and the terminals 1 and 2 of the circuit are connected to an external load R_L.

The thermal efficiency, η_g, of the circuit shown in figure (2.1) can be defined as [15],

$$\eta_g = \frac{P}{q_h}, \tag{2.1}$$

where P is the electrical power delivered to the external load R_L and q_h is the heat input required to maintain the hot junction temperature at T_h.

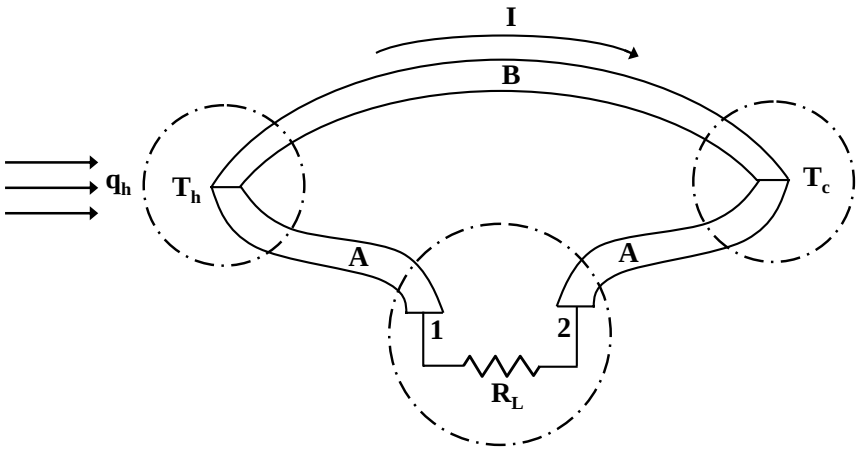

Figure 2.1: Thermoelectric circuit

The electrical power, P, is defined as [15],

$$P \;=\; I^2 R_L. \tag{2.2}$$

I in equation (2.2) is the current flowing through the circuit and is defined as the ratio of emf generated across the circuit to the total resistance of the circuit [15],

$$I \;=\; \frac{\alpha \triangle T}{R + R_L}, \tag{2.3}$$

where α is the combined Seebeck coefficient of the materials A and B, $\triangle T$ is the temperature difference between the hot and cold junctions and R is the total electrical resistance of the materials A and B.

The heat input at the hot junction, T_h, is given by [15],

$$q_h \;=\; K \triangle T + \alpha T_h I - \frac{1}{2} I^2 R, \tag{2.4}$$

where K is the combined thermal conductance of the materials A and B. The terms

$(K\triangle T)$ and $(-\frac{1}{2}I^2R)$ in equation (2.4) result from the two irreversible effects of heat transfer due to thermal conduction and Joule heating. While the term $(\alpha T_h I)$ is due to the reversible Peltier effect.

Combining equations (2.2), (2.3), (2.4), and $(m = \frac{R_L}{R})$ η_g defined in equation (2.1) can be expanded as,

$$\eta_g = \frac{m\left(\frac{\triangle T}{T_h}\right)}{\left(\frac{1+m^2}{T_h}\right)\left(\frac{RK}{\alpha^2}\right) + (m+1) - \frac{1}{2}\frac{\triangle T}{T_h}}. \tag{2.5}$$

For a fixed T_h, T_c, and m, the η_g can be maximized when the term $(\frac{RK}{\alpha^2})$ in the denominator of equation (2.5) is minimized. This grouping of properties, called the thermoelectric figure of merit (Z), is defined as,

$$Z = \frac{\alpha^2}{RK}. \tag{2.6}$$

The higher the Z value, the greater the η_g of the circuit. The α, R, and K of the device or generator are defined as,

$$\left.\begin{aligned} \alpha &= N_c\left(\bar{\alpha}_p - \bar{\alpha}_n\right) \\ R &= N_c\gamma\left(\bar{\rho}_n + \bar{\rho}_p\right) \\ K &= \frac{N_c}{\gamma}\left(\bar{k}_n + \bar{k}_p\right) \end{aligned}\right\}, \tag{2.7}$$

where N_c is the number of (series-connected) couples in the device or generator, $\bar{\alpha}_n$ and $\bar{\alpha}_p$ are the Seebeck coefficients of the n and p type material averaged over the the temperature range T_c to T_h. $\bar{\rho}_n$ and $\bar{\rho}_p$ are the electrical resistivities and $\bar{k}_n$ and $\bar{k}_p$ are the thermal conductivities averaged similarly. γ is the aspect ratio of the legs and assumed uniform over the device or generator. The γ is defined as, $\frac{l_l}{A_l}$, where l_l is the length of the thermoelectric leg and A_l is the cross-sectional area of the leg.

Combining equations (2.6) and (2.7) the Z for the device or generator is equivalent to z, the material figure of merit. The z is defined as [16],

$$z = \frac{\alpha^2}{\rho k}, \tag{2.8}$$

where α is the Seebeck coefficient of the material, ρ is the electrical resistivity of the material, and k is the thermal conductivity of the material. Better thermoelectric materials have high z values. Although, η_g is a function of the Z, ZT would be a better criteria in the design of thermoelectric materials [16]. ZT is defined as,

$$ZT = \frac{\alpha^2}{RK}T, \tag{2.9}$$

where T is evaluated as: $\frac{T_h+T_c}{2}$.

The properties $\bar{\alpha}_n$, $\bar{\alpha}_p$, $\bar{k}_n$, and $\bar{k}_p$ in equation set (2.7) are evaluated by the following expression [15],

$$\bar{x} \equiv \left(\frac{1}{\Delta T_j}\right) \int_{T_{c,j}}^{T_{h,j}} x\left(T\right) dT, \tag{2.10}$$

where $\bar{x}$ represents $\bar{\alpha}_n$, $\bar{\alpha}_p$, $\bar{k}_n$, and $\bar{k}_p$, ΔT_j is defined as, $(T_{h,j} - T_{c,j})$, and $x\left(T\right)$ represents the variation of the n and p-type material properties, α, ρ, and k as a function of temperature. The properties $\bar{\rho}_n$ and $\bar{\rho}_p$ in equation set (2.7) are evaluated as follows,

$$\bar{\rho} = \left(\frac{1}{\bar{k}\Delta T_j}\right) \int_{T_{c,j}}^{T_{h,j}} \rho\left(T\right) k\left(T\right) dT. \tag{2.11}$$

These averages are defined such that when $I = 0$, the voltage predicted by the average equations is equivalent to that obtained by considering property variations with temperature [16].

2.2 Thermoelectric Modules

In this section a description and functionality of the constituents of the thermoelectric modules are discussed. The modules are the basic building blocks within thermoelectric power generators or coolers. Modules are a matrix of semiconductor thermoelectric couples that are connected electrically in series and thermally in parallel. The thermoelectric couples and their electrical interconnects are sandwiched between two ceramic substrates.

Figure (2.2) shows the arrangement of the different constituents of a thermoelectric module. The main constituents of a thermoelectric module are (1) thermoelectric elements (or legs), (2) ceramic substrates, (3) metal interconnects, and (4) external electrical connections.

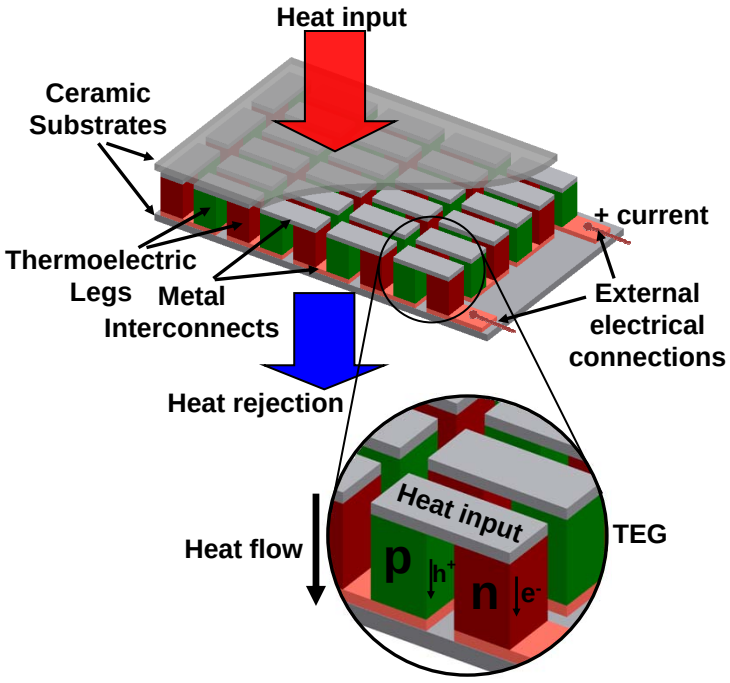

Figure 2.2: Constituents of a thermoelectric module

The thermoelectric elements (or legs) are the couples used for generating electricity in thermoelectric modules. They are formed out of materials such as bismuth-telluride, lead-telluride, antimony telluride, silicon-germanium semiconductor alloys. The selection of material depends on the field of application and operating temperature range. The thermoelectric legs are arranged in a regular matrix within the module, as shown in figure (2.2).

Ceramic substrates are used to electrically insulate the thermoelectric module from external mounting surfaces. The substrates must also have good thermal conductance to provide heat transfer with minimal thermal resistance. A common ceramic substrate is aluminium oxide (Al_2O_3).

The metal interconnects serves as electrical contacts between thermoelectric legs. The contacts are arranged in such a way that all the legs are connected electrically in series.

External electrical connections are used to connect the module to an electrical load in case of power generation or to an electrical source in case of the module being used for thermoelectric cooling.

The thermoelectric modules in conjunction with heat exchangers are used to build systems for TPG. The design features of such a system are discussed in the subsequent section.

2.3 TEG System

In this section an overview of the key design aspects of TEG system for TPG are discussed. Figure (2.3) shows the side view and end view of a typical TEG system. This particular design was based on an actual prototype generator designed and

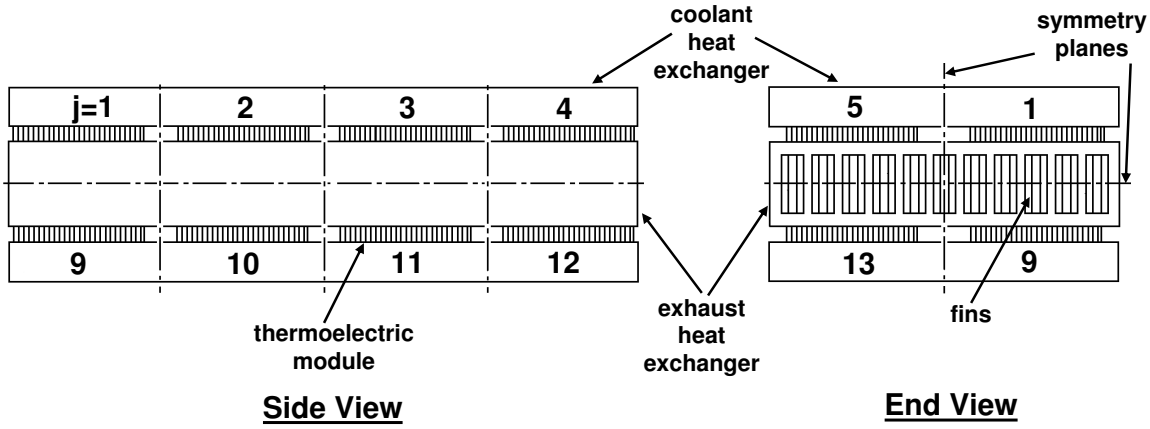

Figure 2.3: Prototype TEG system

built in conjunction with Hi-Z Technology Inc (Hi-Z) [17]. The prototype generator was tested in a 1999 General Motors Sierra pick-up truck [11]. As shown in figure (2.3), the tested generator incorporated HZ20, Bi_2Te_3 based, thermoelectric modules manufactured by Hi-Z. A total of sixteen modules, eight on either side of the central exhaust heat exchanger (EHX), were all connected in series electrically. The EHX was made of carbon steel. Cooling was provided by a pair of aluminum heat exchangers, one on each side of EHX. Thin aluminum oxide wafers electrically isolated the thermoelectric modules from the heat exchangers. The carefully-smoothed contact surfaces on each side of these wafers were covered with thermal grease and the entire assembly was clamped together with a 200 psi cold preload. The exhaust and coolant flow streams orientation is such that it resulted in a counter flow arrangement. A complete description of the prototype TEG system is discussed in [11].

2.4 TEG Simulator

A numerical model of the TEG system will be an effective tool to perform various parametric and system optimization studies. In this section the modeling of a generic TEG system is described. The numerical model framework is based on the prototype TEG system design, discussed in the preceding section.

2.4.1 Simulator Design and Modeling

Figure (2.4) shows the system design of the generic simulator. The device model is

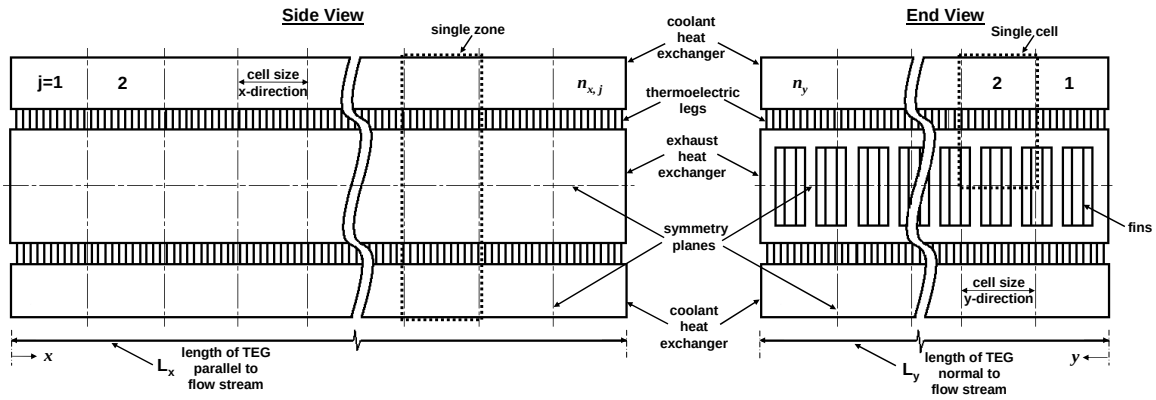

Figure 2.4: TEG Model Layout

based on the following preliminary assumptions: (1) thermal symmetry with respect to the mid planes, and solution uniformity in the horizontal plane as shown in figure (2.4), (2) perfectly insulated heat exchangers and consequently no extraneous heat losses, (3) perfectly insulated cavities or gaps between the thermoelectric legs and therefore no heat transfer due to conduction, convection, or radiation between the legs, and (4) negligible thermal and electrical resistance of the metal interconnects connecting the n and p-type legs. From figure (2.4), the symmetry planes divide the generator into n_x equal sized zones extending over its length parallel to the exhaust

and coolant flow streams. Each zone contains $2 \times n_y$ cells of equal-sized sections containing thermoelectric couples, as shown in figure (2.5). As a result, N_m $(= 2n_x n_y)$

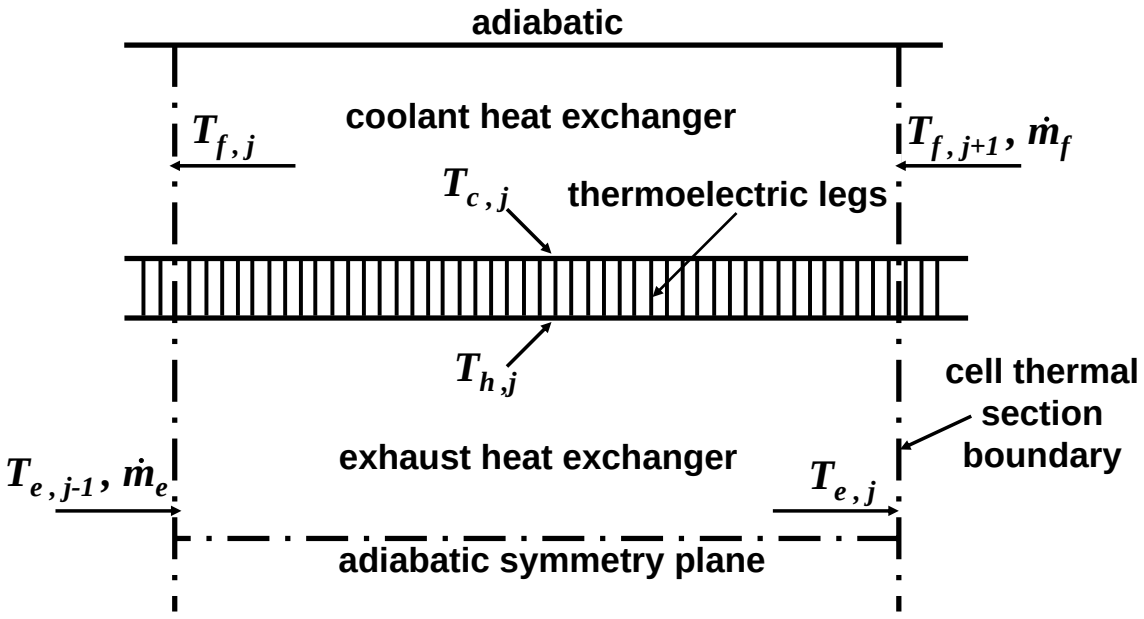

Figure 2.5: Side view of a thermal section j

sections constitute the complete TEG system shown in figure (2.4).

It is assumed all the sections in the TEG system consists of an equal number of thermoelectric couples and also assumed all the thermoelectric couples in a given section are connected in series electrically and together constitute a single thermoelectric module, here after referred to as the module. Furthermore, all the N_m modules in the TEG system are connected in series electrically.

To model the thermal section j shown in figure (2.5), it is assumed the axial conduction in the metal is negligible and that the junction temperatures: $T_{h,j}$ and $T_{c,j}$, are uniform within the module . A steady-state energy balance on the coolant heat exchanger (CHX) section considering convection in the fluid and conduction heat transfer to the module surface gives,

$$c_{p_{f,j}} T_{f,j} - c_{p_{f,j+1}} T_{f,j+1} - \frac{\overline{U}_{f,j} A_{f,j}}{\dot{m}_{f,j}} \left(T_{c,j} - \overline{T}_{f,j} \right) \;=\; 0, \tag{2.12}$$

where $\overline{U}_{f,j}$ is the average overall heat transfer coefficient for the CHX for this section, $A_{f,j}$ is the coolant side heat transfer area for this section, $\dot{m}_{f,j}$ is the mass flow rate of the coolant through the section, $c_{p_{f,j}}$ and $c_{p_{f,j+1}}$ are the specific heat of the coolant evaluated at $T_{f,j}$ and $T_{f,j+1}$, $T_{c,j}$ is the uniform cold junction temperature of the module j, and $\overline{T}_{f,j}$ is the average bulk temperature of the coolant for this section. $\overline{T}_{f,j}$ is defined as,

$$\overline{T}_{f,j} \;=\; \frac{1}{2} \left(T_{f,j} + T_{f,j+1} \right). \tag{2.13}$$

Similarly, for the EHX segment,

$$c_{p_{e,j}} T_{e,j} - c_{p_{e,j-1}} T_{e,j-1} - \frac{\overline{U}_{e,j} A_{e,j}}{\dot{m}_{e,j}} \left(\overline{T}_{e,j} - T_{h,j} \right) \;=\; 0, \tag{2.14}$$

where the variables have definitions similar to those in equation (2.12), and

$$\overline{T}_{e,j} \;=\; \frac{1}{2} \left(T_{e,j} + T_{e,j-1} \right). \tag{2.15}$$

Balancing the energy flow in and out of the module gives,

$$\overline{U}_{e,j} A_{e,j} \left(\overline{T}_{e,j} - T_{h,j} \right) - \overline{U}_{f,j} A_{f,j} \left(T_{c,j} - \overline{T}_{f,j} \right) - P_j \;=\; 0. \tag{2.16}$$

P_j, the power generated by the module is,

$$P_j \;=\; IV_j \;=\; I(V_{oc,j} - IR_j), \tag{2.17}$$

where I is the total current of the generator, $V_{oc,j}$ is the module's open circuit voltage, and R_j is the electrical resistance of the module.

R_j, the electrical resistance of the module is defined as,

$$R_j \;=\; N_{c,j}\gamma\left(\bar{\rho}_n + \bar{\rho}_p\right), \tag{2.18}$$

where $N_{c,j}$ is the number of (series-connected) couples in the module. The γ of the legs is assumed uniform over the generator.

The number of couples in the module, $N_{c,j}$, is defined as,

$$N_{c,j} \;=\; \zeta A_{xy,j}, \tag{2.19}$$

where ζ is the couple density and $A_{xy,j}$ is the plan area of the thermal section j, product of cell size in x-direction and cell size in y-direction, figure (2.4). The total number of couples, N_c, in the TEG is given by $2\zeta A_{xy}$, where $A_{xy} = L_x L_y$ and the factor of 2 for the couples on either side of the EHX. L_x is the length of TEG parallel to the flow stream and L_y is the length of TEG normal to the flow stream.

The module's open circuit voltage, $V_{oc,j}$, is defined as,

$$V_{oc,j} \;=\; \alpha_j\left(T_{h,j} - T_{c,j}\right), \tag{2.20}$$

where α_j is the Seebeck coefficient of the module. α_j is defined as:

$$\alpha_j \;=\; N_{c,j}\left(\bar{\alpha}_p - \bar{\alpha}_n\right). \tag{2.21}$$

The total current of the generator, I, is defined as,

$$I \;=\; \frac{V_{oc}}{R_g + R_L} \;=\; \frac{\sum_{j=1}^{N_m} V_{oc,j}}{\sum_{j=1}^{N_m} R_j + R_L}, \tag{2.22}$$

where V_{oc} is the total open circuit voltage of the generator, R_g is the total electrical resistance of the generator, R_L is the load resistance.

A heat balance at the hot junction of the module as derived in [15] is,

$$\overline{U}_{e,j} A_e \left(\overline{T}_{e,j} - T_{h,j}\right) - K_j \left(T_{h,j} - T_{c,j}\right) - \alpha_j T_{h,j} I + \frac{1}{2} I^2 R_j \;=\; 0, \tag{2.23}$$

where K_j is the thermal conductance of the module. K_j is defined as,

$$K_j \;=\; \frac{N_{c,j}}{\gamma} \left(\bar{k}_n + \bar{k}_p\right). \tag{2.24}$$

Finally, the power of the generator is,

$$P_g \;=\; I^2 R_L. \tag{2.25}$$

2.4.2 Solution Strategy

Referring to figure (2.4), due to horizontal symmetry, all the cells in a given zone have the identical temperature profile. As a result, the temperature profile of a single cell from each zone is determined to establish the temperature profile of the complete generator. Equations (2.12), (2.14), (2.16), (2.17), and (2.23) combined with equation (2.22), were simultaneously solved by the multi-dimensional Newton-Rhapson method to find the four unknown temperatures in each section, $T_{c,j}$, $T_{h,j}$, $T_{e,j}$, $T_{f,j}$, $j = 1, 2, ..., n_x$, and thus also to calculate the performance of the generator, principally its power production. The analysis is carried out at matched load, $R_L = R_g$. The multi-dimensional Newton-Rhapson method is defined as:

$$\vec{x}_{n+1} = \vec{x}_n - \left[F'\left(\vec{x}_n\right)\right]^{-1} F\left(\vec{x}_n\right), \tag{2.26}$$

where $\vec{x}$ is the vector of unknowns: $T_{c,j}$, $T_{h,j}$, $T_{e,j}$, $T_{f,j}$, $j = 1, 2, ..., n_x$, $F\left(\vec{x}\right)$ is the residue vector defined by the equations (2.12), (2.14), (2.16), and (2.23). $F'\left(\vec{x}\right)$ for the TEG model is defined as follows:

$$F'\left(\vec{x}\right) = J_F\left(\vec{x}\right) + \left(\frac{\partial F\left(\vec{x}\right)}{\partial I}\right)\left(\frac{\partial I}{\partial \vec{x}}\right) \tag{2.27}$$

where $J_F\left(\vec{x}\right)$ is the Jacobian of $F\left(\vec{x}\right)$ with respect to the temperature unknowns. This approach was iterated until the absolute change in the temperature unknowns between successive iterations was less than 10^{-3} K, at which point the solution was considered to be converged.

2.5 Material Properties and Design Data

The thermoelectric material properties, fluid properties, and heat exchanger performance data are needed by the model of the TEG. Therefore, in the following material and fluid properties as well as the heat exchanger designs and performance are reported and reviewed.

2.5.1 Thermoelectric Material Properties

A key objective in performing the optimization studies is to make a comparative study of the variation in the design and performance of the TEG due to the change in thermoelectric material from commercially available low zT bulk materials to recently available high zT materials. Bi_2Te_3 was selected to represent the commercially available low zT material and quantum well structured (QW) B_4/B_9C (QW p-type) and Si/SiGe (QW n-type), was selected to represent the recently available high zT materials. In the following a comparison of the thermoelectric material properties, α, ρ, and k, between the QW and the conventional Bi_2Te_3 materials is given. The material properties were furnished by Hi-Z [19, 20]. Figure (2.6) shows a comparison of α between the QW and the Bi_2Te_3 materials. The α for the QW material was greater than that of the Bi_2Te_3 material by a factor of 5.6 to 7.6 for the n-type and 5 to 6 for the p-type.

Figure (2.7) shows a comparison of ρ between the QW and the Bi_2Te_3 materials. The difference in resistivity between the n and p-type QW at lower temperature is marginal and increases proportional to the temperature. In contrast, resistivities of the n and p-type Bi_2Te_3 materials are approximately of equal magnitude at any given temperature However, both the n and p-type Bi_2Te_3 resistivities increase proportional to the temperature. The combined resistance of the n and p-type legs for the Bi_2Te_3

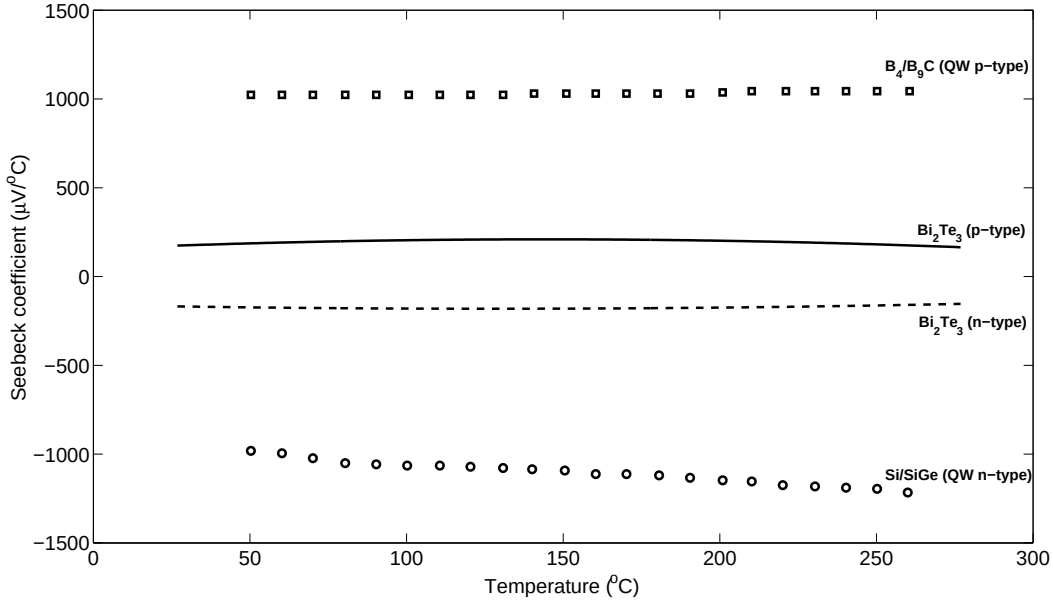

Figure 2.6: QW and Bi_2Te_3 material Seebeck coefficients

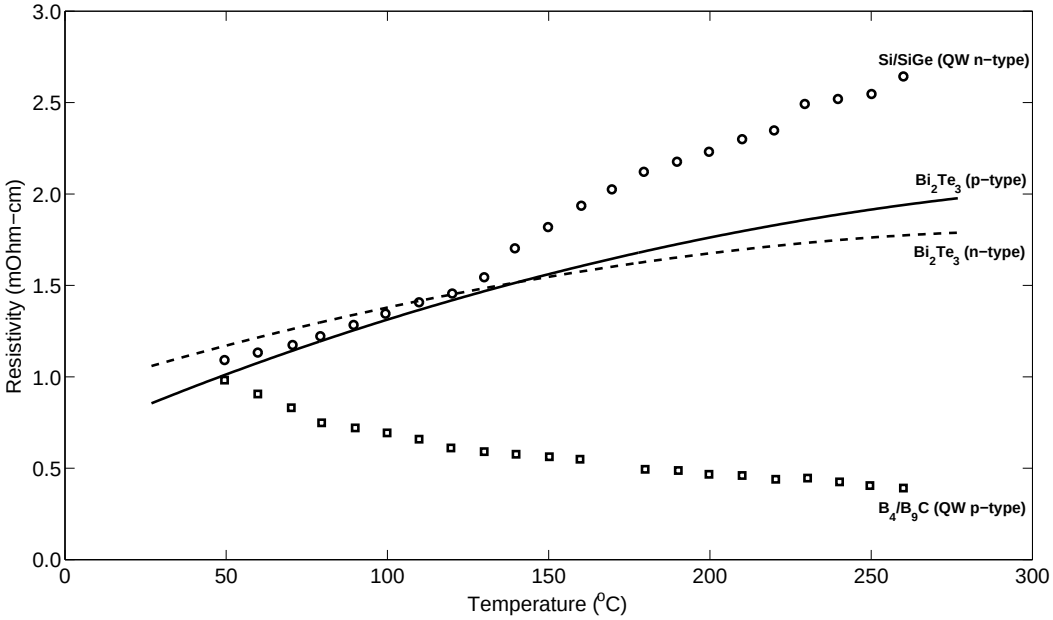

Figure 2.7: QW and Bi_2Te_3 material electrical resistivities

couple was greater than the QW couple by a factor of 1.3.

Figure (2.8) shows a comparison of k between the QW and the Bi_2Te_3 materials.

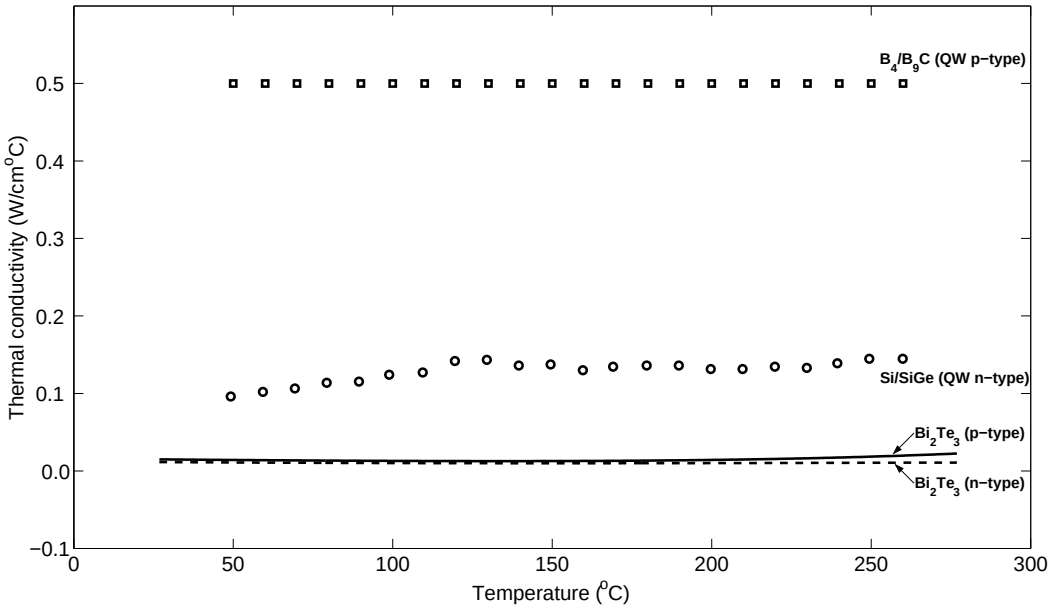

Figure 2.8: QW and Bi_2Te_3 material thermal conductivities

As shown in figure (2.8), there is a substantial difference in the magnitude of k between the n and p-type QW materials. In contrast, the difference between the n and p-type Bi_2Te_3 k is marginal. Furthermore, the k of the n and p-type QW material are higher than the n and p-type Bi_2Te_3 material. The ratio of n-type QW to that of the n-type Bi_2Te_3 varies approximately between 9 to 14. In comparison, the ratio of p-type QW to that of the p-type Bi_2Te_3 varied approximately between 25 to 39. Figure (2.8) also shows that there is no variation of k as a function of temperature for all of the n and p-type materials, except for the marginal variation of the n-type QW material.

Figure (2.9) compares the zT of QW and Bi_2Te_3 materials. A comparison of the ZT of QW and Bi_2Te_3 modules, for the identical γ and equal N_c, is shown in figure (2.10). The ZT enhanced by a factor of 1.4 to 2 between the QW and Bi_2Te_3 modules. Using these material properties, the module properties R_j, α_j, and K_j in

equations (2.17), (2.20), and (2.23), are evaluated using equations (2.18), (2.21), and (2.24) respectively.

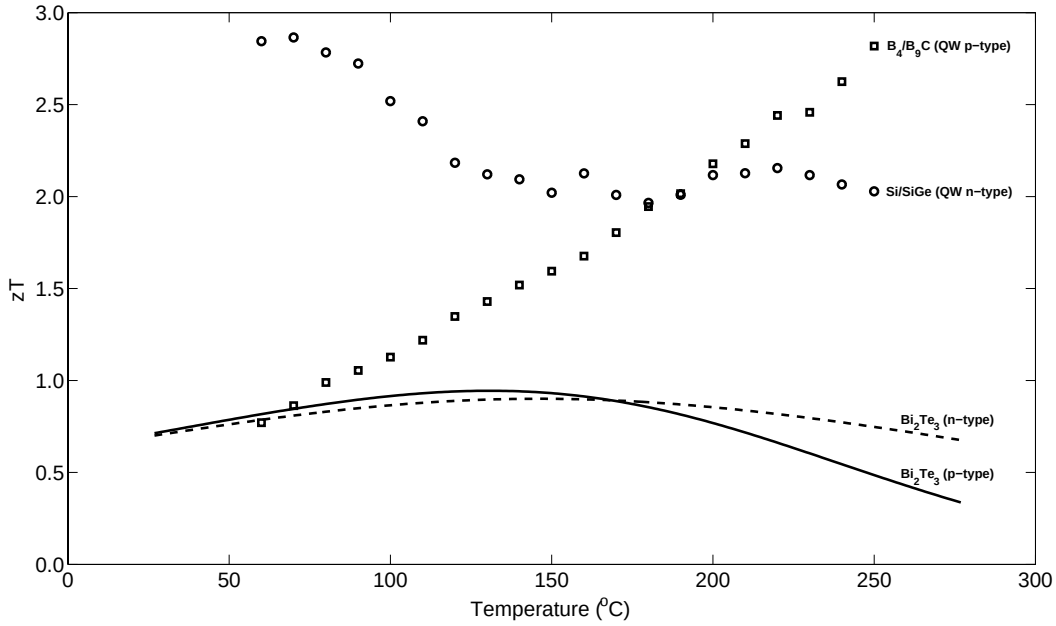

Figure 2.9: QW and Bi_2Te_3 material zT

2.5.2 Fluid Properties

The fluid properties are evaluated as a function of temperature. The density (ρ_e) and specific heat (c_{p_e}) at constant pressure of the exhaust gas are found from ideal gas mixture theory [21]. The relative amounts of pure components in the exhaust mixture are determined using molar analysis for a given fuel type and the air to fuel mass ratio. The dynamic viscosity of the gas is found using an equation for gas mixtures [22]. For the coolant properties in mobile application, an engine coolant composed of 50% by volume solution of ethylene glycol in water, was used to cool the TEG and the properties are evaluated using the Prestone Antifreeze coolant properties [23]. In the stationary application, water was used to cool the TEG. Its properties are assumed

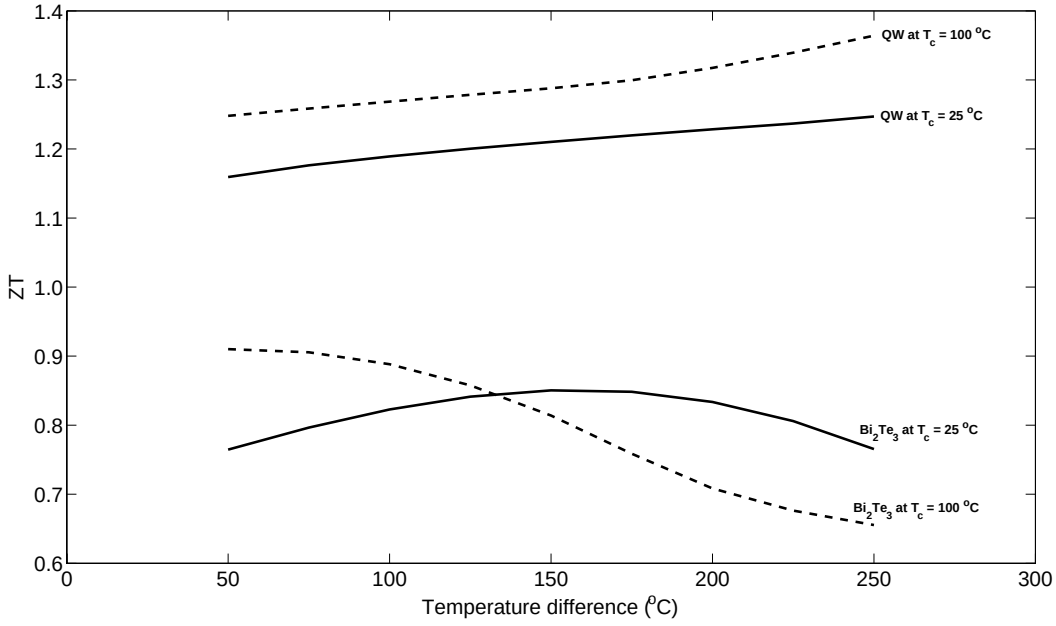

Figure 2.10: A comparison of QW and Bi_2Te_3 ZT

to be those of liquid water at a pressure of 100 (kPa).

2.5.3 Heat Exchangers and Heat Transfer Coefficients

The overall heat transfer coefficients, $\overline{U}_e$ and $\overline{U}_f$, included the forced convective heat transfer coefficients in the heat exchangers, the conduction through the fins, and the contact resistance between the heat exchangers and the thermoelectric modules. The heat exchanger surface geometry, especially the plate fin surfaces [24], are characterized by the following design parameters:

- Plate spacing, b
- Flow length of uninterrupted fin, L
- Fin thickness, δ
- Fin spacing, s

- Fins per unit length normal to flow direction, fin pitch (FP)
- Hydraulic diameter, $4r_h$. It is defined as $4L\frac{A_c}{A}$, where A_c is the flow cross-sectional area and A is the heat transfer area. A is defined as $(A_f + A_b)$, where A_f is the fin surface area and A_b is the prime surface area or exposed portion of the base [25]
- Ratio of heat transfer area to fin area, $\frac{A}{A_f}$
- Heat transfer area per unit volume between plates, $\beta = \frac{A}{V}$

A few of the above listed characteristics are shown in figures illustrating the designs of EHX and CHX.

Exhaust Heat Exchanger

The EHX is an offset-strip fin design, shown in figure (2.11). This particular design

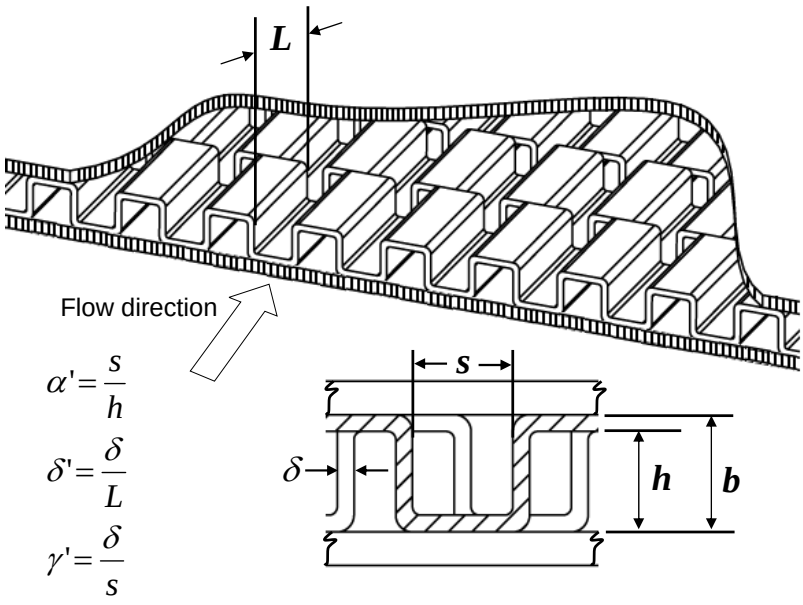

Figure 2.11: EHX design, rectangular offset strip fin array

was selected based on its prior usage in the TPG experimental [11] and performance studies [26]. The design characteristics of this surface geometry are listed in table (2.1).

Table 2.1: EGHX surface geometry design characteristics

b (mm)	FP $\left(\frac{1}{\text{m}}\right)$	$4r_h$ (mm)	δ (mm)	s (mm)	L (mm)	β $\left(\frac{1}{\text{m}}\right)$	$\frac{A}{A_f}$
31.75	65	16.6	4.57	12	76.2	174.3	0.746

This design is close to that for which correlations for the Colburn factor, $j = \frac{Nu}{RePr^{\frac{1}{3}}}$, and friction factor, $f = \frac{\rho\tau}{\left(\frac{\dot{m}}{A_c}\right)^2}$, were reported in [27] to agree with experimental data to within 20% for a range of fin geometry. Where Nu is the Nusselt number defined as the ratio of convective heat transfer to conductive heat transfer, Re is the Reynolds number defined as the ratio of inertia force to viscous force, Pr is the Prandtl number defined as the ratio of momentum diffusivity to thermal diffusivity, ρ is density of the fluid, τ is unit surface shear stress, and $\dot{m}$ is mass flow rate of the fluid. The Colburn factor correlation was defined as,

$$\begin{aligned} j &= 0.6522Re^{-0.5403}\alpha'^{-0.1541}\delta'^{\ 0.1499}\gamma'^{-0.0678} \\ &\quad \left\{1 + 5.269 \times 10^{-5}Re^{1.34}\alpha'^{0.504}\delta'^{\ 0.456}\gamma'^{-1.055}\right\}^{0.1}, \end{aligned} \tag{2.28}$$

where α', δ', and γ' are dimensionless ratios of the fin and channel dimensions as shown in figure (2.11). The Reynolds number was defined based on the hydraulic diameter of a unit fin channel of the offset-strip fin array. The friction factor correlation was dependent upon the same variables and was defined as,

$$\begin{aligned} f &= 9.6243Re^{-0.7422}\alpha'^{-0.1856}\delta'^{\ 0.3053}\gamma'^{-0.2659} \\ &\quad \left\{1 + 7.669 \times 10^{-8}Re^{4.429}\alpha'^{0.920}\delta'^{\ 3.767}\gamma'^{0.236}\right\}^{0.1}. \end{aligned} \tag{2.29}$$

Coolant Heat Exchanger

The CHX consisted of parallel rectangular flow channels, as shown in figure (2.12). As was the case with EHX, the CHX design was selected based on its prior usage in

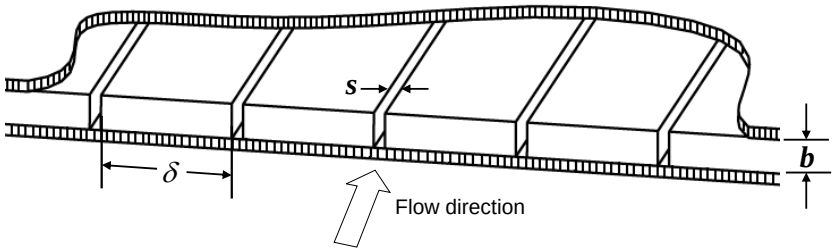

Figure 2.12: CHX design, parallel rectangular flow channels

the TPG experimental [11] and performance studies [26]. The design characteristics of this surface geometry are listed in table (2.2).

Table 2.2: CHX surface geometry design characteristics

b (mm)	FP $\left(\frac{1}{\text{m}}\right)$	$4r_h$ (mm)	δ (mm)	s (mm)	L (mm)	β $\left(\frac{1}{\text{m}}\right)$	$\frac{A}{A_f}$
12.7	37	6	23	4	-	100	0.76

The heat transfer coefficient (h) and pressure drop (Δp) for this design were modeled using the Colburn factor and friction factor data for flow through rectangular channels. Using a combination of analytical and experimental studies, Kays and London [24] performed a comprehensive treatment of gas flow through rectangular channels of aspect ratio, α=3, and with abrupt contraction entrances. The effects of tube length, type of heating, and temperature-dependent fluid properties were also investigated in these studies.

Figure (2.13) shows the data used in estimating the h and Δp of the CHX design listed in table (2.2). Figure (2.13) shows smooth curves for the j and f data. However,

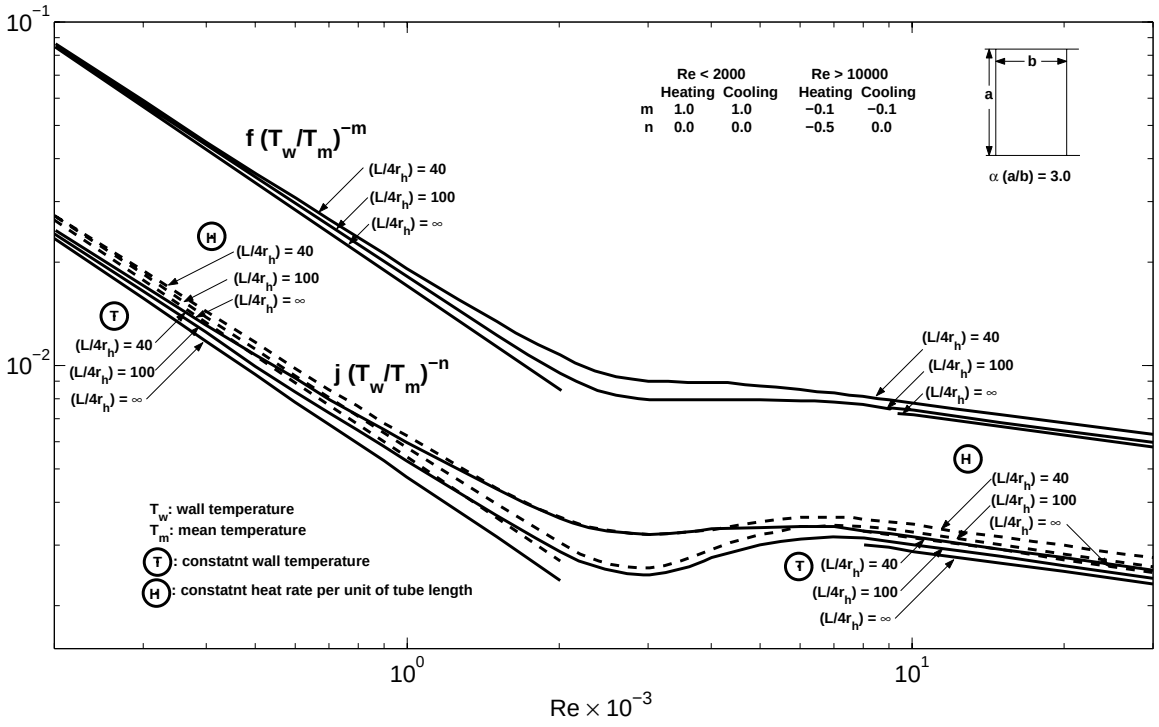

Figure 2.13: Gas flow inside rectangular tubes: a summary of experimental and analytical data [24]

unlike the correlations for j and f of EHX, the j and f data of CHX at any given Re is estimated directly from the data shown in figure (2.13).

The fraction of the exhaust energy not converted to TEG power heats the coolant. The exponents m and n listed in figure (2.13) are chosen accordingly. The ratio $\left(\frac{T_w}{T_m}\right)$ accounts for the temperature dependent fluid properties at a particular flow section, where T_w is the wall temperature ($= T_c$) and T_m is the mean fluid temperature $\left(= \frac{T_{f,j}+T_{f,j+1}}{2}\right)$. From figure (2.13), the variation in the j characteristics between the thermal boundary conditions, constant wall temperature, Ⓣ, and constant heat rate per unit length, Ⓗ, is marginal. In addition, the effect of the dimensionless

tube length, $(L/4r_h)$, on the f and j characteristics is marginal for $Re \leq 2000$ and $Re \geq 10000$. Therefore for $2000 > Re > 10000$, the mean data between the curves corresponding to $L/4r_h = 100$ and $L/4r_h = \infty$ was used in estimating the f and j characteristics of the CHX for any $(L/4r_h)$. Though there is significant effect of $(L/4r_h)$ on the f and j characteristics for the transition regime, a linear interpolation was performed using data at $Re = 2000$ and $Re = 10000$ to determine the f and j for $2000 < Re < 10000$. Nevertheless, this should not give rise to any significant discrepancies, as the actual data itself in the transition regime are subject to considerable uncertainty because of the unstable nature of the transition problem [24]. The Re varied between 180 to 12000 over the complete set of optimization runs.

The data shown in figure (2.13) was specifically developed to estimate the heat transfer coefficient and pressure drop for the gas Prandtl number (Pr) range. However, the two coolant fluids used in this study were ethylene glycol and water, Prandtl number of approximately 7. Therefore, the data shown in figure (2.13) was validated against data from the literature that used rectangular channels of aspect ratio 3 and water as the test fluid. It was observed that the data from Kays and London, figure (2.13), agreed well and can be used to predict the heat transfer coefficient and pressure drop of fluids with Prandtl number of 7.

To summarize the TEG system design was described. This was followed by a description of the TEG system model to determine the temperature distribution and consequently the power. Subsequently, an overview of the fluid and thermoelectric material properties and the design and performance of heat exchangers required by the TEG model was performed. The ZT was enhanced by a factor of 1.4 to 2 between the QW and Bi_2Te_3 modules. Therefore, the enhancement in TEG power between the QW and and Bi_2Te_3 should scale approximately by a factor of 1.4 to 2. Using the previously discussed TEG simulator, parametric and optimization studies were performed on two different applications. The optimization problem statement and a description of the two cases are discussed in the subsequent chapter.

Chapter 3

TPG Optimization and Problem Definition

In the preceding chapter, the design code for the TEG simulator has been developed such that it can predict various combinations of system size, thermoelectric materials, heat exchangers designs, and exhaust and coolant flow stream conditions. Despite this, the previously discussed thermoelectric materials and heat exchanger designs were selected for the parametric and optimization studies. The reasons for this are as follows, (1) the prior usage of selected materials and heat exchanger designs in testing [11] to ensure that the baseline predictions are reasonable and (2) a comparison of the enhancement in the performance of TEG with and without the optimization can be made.

This chapter begins with an overview of the system design of the two case studies. The modeling and optimization approach is discussed subsequently and followed by the definition of the net power and the estimation of various parasitic losses, thus establishing the complete TEG model. Based on the system description of the two case studies and the previously described TEG simulator and modeling approach,

parameters required for the the TPG optimization are classified. Subsequently, the TPG optimization problem is stated and described. The optimization strategy and solver are discussed in the last section.

3.1 Case 1: Sports-Utility Vehicle

In this section the system design for Case 1, a sports-utility vehicle (SUV) is described. Figure (3.1) shows the system layout. This layout was based on the installation

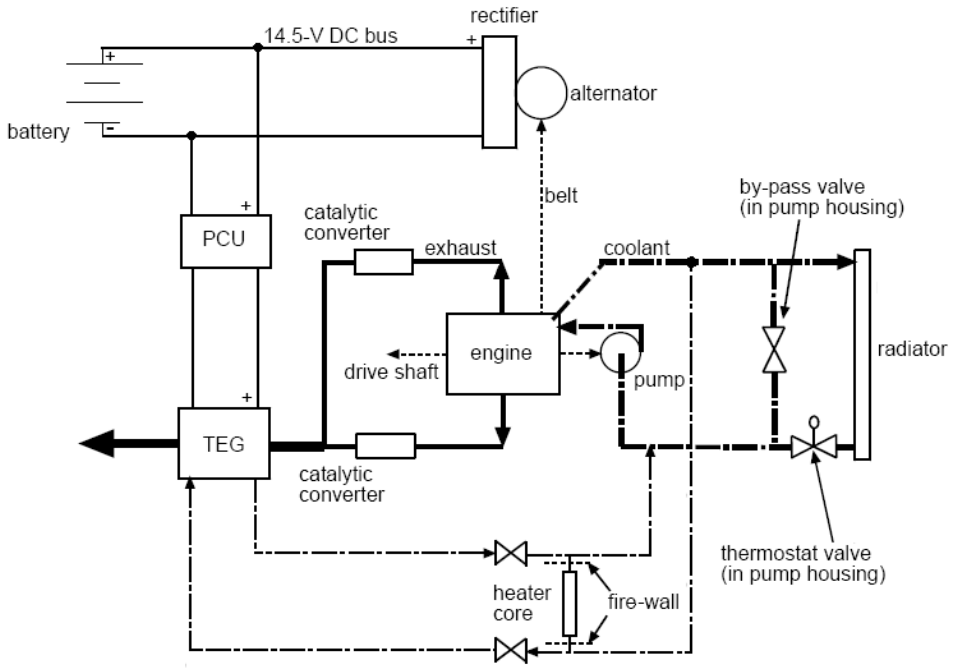

Figure 3.1: System design Case 1

reported in [11] in which the TEG was located downstream of the catalytic converters as shown in figure (3.1) and the intervening exhaust piping was insulated. Vazquez *et al.* [10] and motor vehicle industry contacts advised against locating TEGs between the exhaust manifold and the catalytic converters because of possible slowing of heating of catalytic converters, resulting in an increased pollutant release.

Engine coolant was chosen to cool the TEG instead of air cooling because the larger heat transfer coefficient available with liquid cooling allows smaller heat exchangers to be used and does not require fans at low or zero vehicle speed. As the TEG coolant loop was connected to the engine coolant system through the cabin heat hoses, the temperature of the coolant supplied to the TEG was actually highest in the coolant system. The most desirable point to tap into the coolant system would be just after the radiator because this is the coldest point in the system. However, the operation of the by-pass and thermostat valves could then prevent continuous coolant flow to the TEG.

As shown in figure (3.1), the electrical output of the TEG was connected to the vehicle's electrical bus through a power conditioning unit (PCU). The PCU was essentially a direct-current-to-direct-current converter functioning as a buck regulator. It matched the generator's output voltage to the approximately 14.5 V potential of the vehicle's direct current bus and kept the TEG operating at its maximum power point.

3.2 Case 2: CNG Engine Generator

In this section the system design for Case 2, a stationary, compressed natural gas (CNG) engine-generator is described. Figure (3.1) shows the system layout for Case 2. The CNG engine was a John Deere 8.1 L and 186 kW SI engine. The TEG was located downstream of the catalytic converter for the reasons given earlier in Case 1. It was assumed that there would be a continuous supply of water from the city mains or cooling towers to cool the TEG.

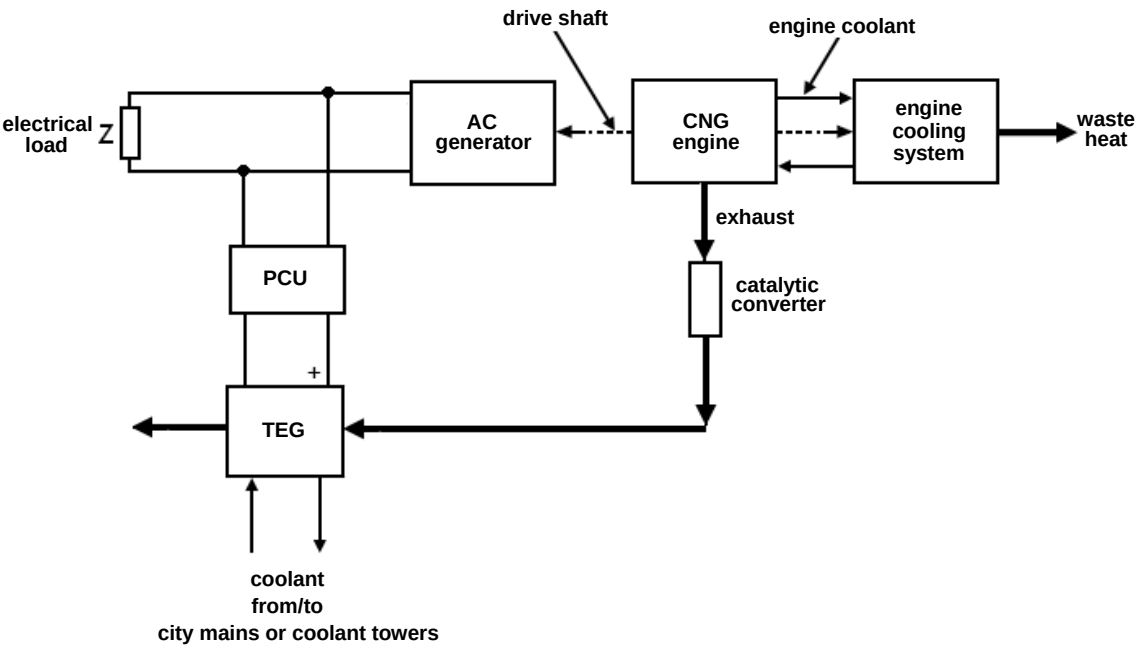

Figure 3.2: System design Case 2

As shown in figure (3.2), the electrical output of the TEG was connected to the alternating-current (AC) generator's electrical bus through a PCU. The PCU for this study, besides matching the TEG output to the AC generator voltage and tracking the maximum power point of the TEG, converts the TEG output from direct to alternating current. The PCU's efficiency was assumed to be 88%. The AC generator performance data was obtained from the specification sheet for the John Deere Power Tech 6068H Diesel engine for generator set applications [36]. This AC generator was chosen based on the load capabilities of the CNG engine. The AC generator electrical output varied between 124 to 143 kW, at a frequency of 60 Hz and an efficiency of about 88 to 92%.

3.3 Modeling and Optimization Approach

In the design of the TEG system, the objective is to maximize the power from the TEG. With the current performance of thermoelectric materials the TEG is more suitable as a system for bottoming cycle [21]. Under such a scenario the objective of TEG system design would be to maximize the combined system efficiency or the net power from the TEG. Therefore the ideal strategy for TEG optimization should be as shown in figure (3.3), by coupling the optimizer, TEG simulator, and the engine

Figure 3.3: Ideal TEG optimization approach

simulator. The engine simulator represents either the vehicle system model in Case 1 or the CNG engine system model in Case 2. The engine simulator would provide parameters such as exhaust flow rate and inlet temperature and coolant flow rate and inlet temperature to the TEG model. The output parameters, TEG power and associated parasitic losses would be fed back to the engine simulator which then would predict the fuel consumption. Such a feed-back coupled system will be able to precisely estimate the exhaust mass flow rate and inlet temperature based on the net gains produced by the TEG. However, running such a coupled system is computationally expensive. Instead, the optimization was performed excluding the engine simulator by using the exhaust mass flow rate and inlet temperature from the baseline (no TEG installed) simulation results.

The optimum design based on baseline flow conditions would deviate from the exact optimum design. However, the resulting change in fuel consumption and flow

conditions due to the current performance of the QW and Bi_2Te_3 materials would be marginal. Thus the TEG optimization based on the baseline flow conditions was performed under the assumption that the resulting optimum design would not deviate significantly from the exact optimum design. The objective of the TEG optimization based on the baseline flow conditions is to maximize the net power from the TEG system. The net power (P_{net}) is defined as:

$$P_{net} = \left(\frac{\eta_{pcu}}{\eta_{aa}}\right) P_g - P_L, \tag{3.1}$$

where η_{pcu} is the PCU efficiency and η_{aa} is the alternator or electrical generator efficiency and P_L is the total parasitic losses. The P_L consists of (1) coolant pumping power, (2) blow down work, and (3) the power to transport the TEG system weight (only for mobile applications). In the following the evaluation of various parasitic losses are discussed.

3.3.1 Coolant Pumping Power

Case 1: In Case 1 the coolant pumping power is based on the model of the coolant system in the truck used for testing the TEG [11]. The model predicts the coolant flow rate through the TEG, the additional pumping power needed to cool the TEG, and the change in flow rates through the other components of the coolant system. The measurements taken during the prototype testing of TEG [11] and additional data supplied by General Motors [35] and [34] were used in the model development and the verification reported by [26]. Figure (3.4) is a flow diagram of the system with resistor symbols representing loss coefficients. The main flow loop is through the pump and engine and then through four parallel paths consisting of the radiator bypass, the radiator, the heater, and the TEG. The model is bi-polar in that it treats

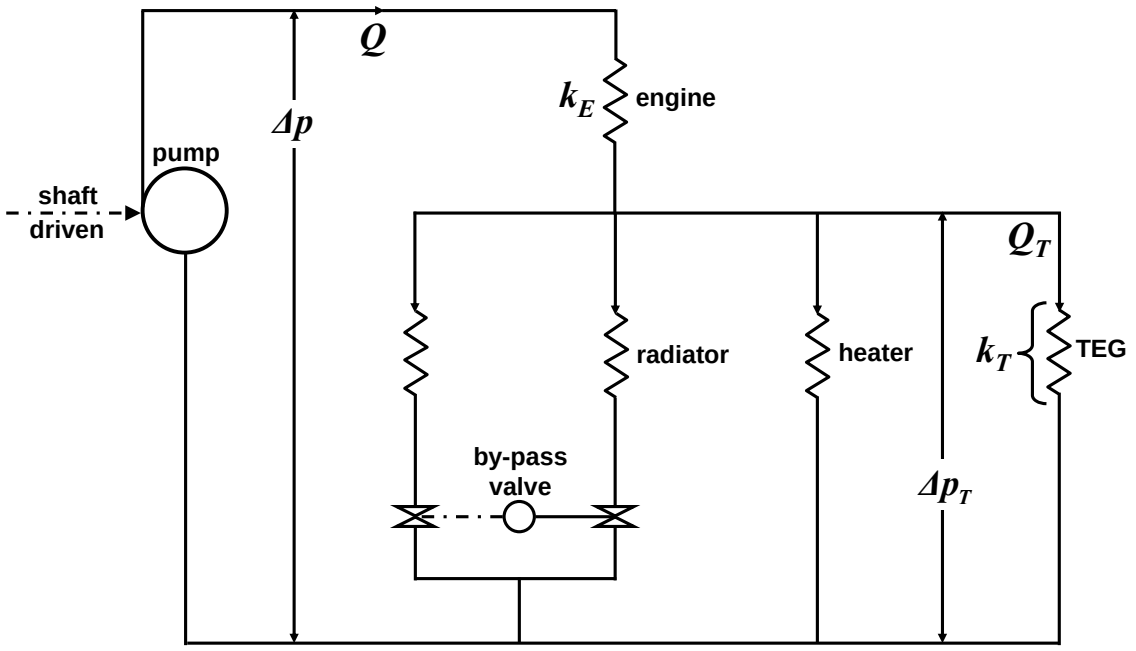

Figure 3.4: Case 1 coolant system circuit

only the case when the thermostat valve is fully open or fully closed. Sufficient data to model the intermediate condition could not be obtained. However, the former condition will exist during cruising at constant speed, the state adopted in Case 1.

The coolant was assumed incompressible and changes in potential and kinetic energy were neglected. The pressure losses for any fluid element, Δp, was assumed to obey

$$\Delta p = \rho_f k Q^2 \tag{3.2}$$

where Q is the volumetric flow rate through the element and ρ_f is the coolant density. The loss coefficients, k, were assumed to depend only on the Reynolds number. Because it was difficult to precisely define the hydraulic diameter and thus the Reynolds number in some locations, the data was fit using the following alternative

form, where ν is the kinematic viscosity,

$$k = C_1 \left(\frac{Q}{\nu} \right)^{C_2}. \tag{3.3}$$

Karri [26], reports the various values of C_1 and C_2 used to fit the experimental data for each flow resistance. Reference [26] showed that equation (3.3) worked well for most flow elements except in the engine case, where the scatter in the data was large. However, the predictions of the system model agreed well with the available measurements.

GM provided data relating engine speed to flow and pressure drop for various components of the unmodified system, but a pump characteristic curve at any given engine speed was not available. Therefore, with the assumption that the flow rates through the TEG would be low relative to the flow rates through the other components of the coolant system, it was assumed that the variation in the pump head caused by the additional flow to the TEG could be neglected.

The loss coefficients of various components in the system were used to determine an equivalent system loss coefficient (k_S) using standard methods [37] and then equation (3.2) was used to determine the total flow through the system. The Δp or the pump head across the four parallel paths: the radiator bypass, the radiator, the heater, and the TEG was then determined by

$$\Delta p_T = \Delta p_P - \rho_f k_E Q^2, \tag{3.4}$$

where Δp_P is the pump pressure rise at a given engine rotational speed, k_E is the loss coefficient of the engine and Q in equation (3.4) is the total flow through the system. Then using the Δp_T and the previously determined loss coefficients the new flow rates through each of the four parallel paths was determined by equation (3.2). This

process was performed iteratively to allow for the variation of the loss coefficients. The pumping power was then estimated as

$$P_P = \frac{\rho_f k_S Q^3}{\eta_P}, \tag{3.5}$$

where Q in equation (3.5) is the total flow through the system and η_P is the coolant pump efficiency. The parasitic coolant pumping power was then estimated as

$$\Delta P_P \;=\; P_P \;-\; P_{P0}, \tag{3.6}$$

where P_{P0} is the pumping power in the baseline case (no TEG) and P_P is the pumping power with the TEG.

Case 2: As Case 2 is an open loop coolant system, it was assumed there was continuous coolant flow to/from the reservoir, the parasitic coolant pumping power increase was estimated by dividing the hydraulic power associated with the TEG circuit by the pump efficiency, as given by equation (3.7).

$$\Delta P_P \;=\; \frac{\rho_f k_T Q_T^3}{\eta_P}, \tag{3.7}$$

where k_T is the loss coefficient of the TEG coolant circuit and Q_T is the TEG coolant flow. However, the η_P in equation (3.7) has not been accounted for, as it was not yet determined what might be the pump characteristics of such a system. The η_P will effect the optimum design parameters. However, it was presumed that there might not be a drastic change in the optimum design parameters as compared to an offset in the net power. The effect of η_P on the optimum design parameters was not investigated in the current work.

It should be noted that, while the pumping power in Case 2 will be explicitly dependent on the system size, L_x and L_y, the pumping power in Case 1 will be rather dependent of the system characteristics of the vehicle coolant system. To further elaborate, in Case 2 the coolant mass flow rate ($\dot{m}_f$) is a function of TEG flow resistance and was assumed the required pump head corresponding to the $\dot{m}_f$ would be generated by modifying the TEG loss coefficient (k_T). For example, in the experimental testing of Case 1 [11], the coolant flow rate was adjusted by opening or closing butterfly valves in the TEG coolant loop. In contrast, in Case 1 the TEG coolant loop was connected across the heater core, figure (3.1). Thus it was assumed the optimum $\dot{m}_f$ would be attained by modifying the k_T based on the head available across the heater core circuit. A similar scheme for Case 1 was implemented during the experimental testing of the prototype TEG [11].

3.3.2 Blow Down Work

The blow-down power is the power required for the engine to drive the exhaust through the exhaust system. This power is supplied directly by the engine and changes because of the flow resistance introduced by the TEG exhaust heat exchanger. Representing the base case by the subscript "0", the blow-down power change caused by the altered exhaust back-pressure can be calculated as

$$\Delta P_B = k_e \frac{\dot{m}_e^3}{\rho_e^2} - k_{e0} \frac{\dot{m}_{e,0}^3}{\rho_{e,0}^2}, \tag{3.8}$$

where ρ_e is the exhaust density and k_e is a lumped exhaust loss coefficient which includes the losses from the exhaust pipes, muffler, catalytic converter, and TEG. A negative or positive change in blowdown work will depend on the relative magnitude of the changes in $\dot{m}_e$ and k_e. If there is a decrease in shaft power due to the gains

produced by the TEG, $\dot{m}_e$ will decrease as a result of the increased fuel efficiency and the blow down work may decrease in spite of the increased k_e. This was observed during the testing reported by [11].

Ideally, $\dot{m}_e$ in equation (3.8), must be estimated by coupling the optimizer, TEG simulator, and the engine simulator, as shown in figure (3.3). As discussed previously, the engine simulator estimates the exhaust mass flow rate, exhaust inlet temperature, fuel consumption, and other parameters based on the torque and speed load conditions of the engine. However, running such a coupled system is computationally expensive. Instead, the optimization was performed excluding the engine simulator by using the $\dot{m}_e$ and the $T_{e,i}$ from the baseline simulation results. The blowdown work is included in the optimization, but this is only through the variation of k_e of the heat exchanger design. One could perceive this as being an optimization where the power of the TEG is not fed-back to reduce the engine load, but rather used to support additional electrical loads in the vehicle.

In addition, due to the lack of exhaust system loss coefficient data, the baseline blow down work ($k_{e0}\frac{\dot{m}_{e,0}^3}{\rho_{e,0}^2}$) was neglected. However, this should not alter the optimum design, as the baseline blow down work is independent of the design variables and remains constant. Nevertheless, the P_{net} over the complete design space is offset by the magnitude of $k_{e0}\frac{\dot{m}_{e,0}^3}{\rho_{e,0}^2}$.

3.3.3 Power to Transport TEG System Weight

The parasitic power to transport the total weight of the TEG system is given by

$$\Delta P_D = \frac{\mu_D W_T v}{\eta_D}, \tag{3.9}$$

where μ_D is the rolling resistance coefficient, W_T is the weight of the TEG system, v is the velocity of the vehicle, and η_D is the driveline transmission efficiency. The driveline transmission efficiency accounts for the losses in the linkages between the drive shaft and the wheels and is a function of vehicle speed. Equation (3.9) is valid only at constant speed and zero grade.

3.4 TPG Governing Parameters

Based on the previously described TEG and optimization models, the governing parameters for a complete TPG optimization problem are identified and the key input, design, and constraint variables are listed below:

Input variables

- Heat source
  - Heat source characteristics
    - Exhaust gas composition
    - Inlet temperature ($T_{e,i}$)
    - Mass flow rate ($\dot{m}_e$)
  - Heat exchanger characteristics
    - Material data - ρ and k
- Heat sink
  - Heat sink characteristics
    - Inlet temperature ($T_{f,i}$)
  - Heat exchanger characterisitics

    * Material data - ρ and k

- Thermoelectric materials properties
  - $\alpha(T)$, $\rho(T)$, and $k(T)$
- Data to estimate the coolant pumping power
  - As discussed in section (3.3.1), coolant system characteristics such as loss coefficients of various coolant system components, pump head, and pump efficiency are required to estimate the additional coolant pumping power. In the current studies the inputs required to estimate the coolant pumping power was implemented through the coolant system model
- Data to estimate the blow down work
  - Similar to the coolant pumping power, data such as the exhaust mass flow rate and exhaust system loss coefficients are necessary to estimate the blow down work. As discussed in section (3.3), the exhaust mass flow rate is obtained from the vehicle system model in Case 1 and the engine system model in Case 2. The vehicle system model or the engine system model estimates the exhaust mass flow rate through either the engine efficiency map or fuel consumption map as function of engine rotational speed and torque output at the engine shaft
- Data to estimate the power required to transport the TEG weight
  - As discussed in section (3.3.3), the data necessary to estimate this parasitic loss is rolling resistance coefficient, weight of the TEG system, vehicle speed, and driveline efficiency

Auxiliary data and relations

- Heat source
  - Heat source characteristics
    - Fluid properties - density (ρ_e), specific heat (c_{p_e}), thermal conductivity (k_e), and viscosity (μ_e)
  - Heat exchanger characteristics
    - Performance data - Colburn factor, $j\,(Re)$ and friction factor, $f\,(Re)$
- Heat sink
  - Heat sink characteristics
    - Fluid properties - density (ρ_f), specific heat $\left(c_{p_f}\right)$, thermal conductivity (k_f), and viscosity (μ_f)
  - Heat exchanger characteristics
    - Performance data - Colburn factor, $j\,(Re)$ and friction factor, $f\,(Re)$

Design variables

- Heat source
  - Heat exchanger characteristics
    - Flow configuration - fin type, fin pitch, fin spacing (s), fin length (L), and fin thickness (δ)
    - EHX size - length parallel to the flow stream (L_x), length normal to the flow stream (L_y), and plate spacing (b)

- Heat sink
  - Mass flow rate ($\dot{m}_f$)
  - Heat exchanger characteristics
    * Flow configuration - fin type, fin pitch, fin spacing (s), fin length (L), and fin thickness (δ)
    * CHX size - length parallel to the flow stream (L_x), length normal to the flow stream (L_y), and plate spacing (b)
- Thermoelectric legs and couples - cross-sectional area of the leg (A_l), length of the leg (l_l), and couple density (ζ)

Variables with constraints

All the previously listed design variables are either bounded or constrained to satisfy a combination of physical, material, or economic constraints. The bounding of the design variables pertains to the range of each of the design variable within which the optimum is determined. The constraints pertains to satisfying a combination of linear and non-linear relationships between one or more design or auxiliary variables. In the following such linear and non-linear constraints are listed below.

- Maximum allowable hot junction temperature, $T_h < T_{h,max}$
- Total area of all the thermoelectric legs on either side of the EHX should not exceed the planar area of the TEG system, $N_c A_l \leq L_x L_y$
- Length of EHX parallel to the flow stream must be equal to the length of CHX parallel to the flow stream, $\text{EHX}\,(L_x) = \text{CHX}\,(L_x)$. Similarly, Length of EHX normal to the flow stream must be equal to the length of CHX normal to the flow stream, $\text{EHX}\,(L_y) = \text{CHX}\,(L_y)$

3.5 Optimization: Design Variables

For this work, we limit the study to a subset of the entire space of design variables. The design variables investigated in this work are listed below,

- Length of TEG parallel to the exhaust and coolant flow streams, L_x,
- Length of TEG normal to the exhaust and coolant flow streams, L_y,
- Coolant mass flow rate, $\dot{m}_f$,
- Thermoelectric couple density (per unit area), ζ, and
- Aspect ratio of the thermoelectric leg, γ.

A comparison of the above listed design variables to the previously listed design variables shows that a more comprehensive optimization could have been attempted by including parameters such as thermoelectric materials, heat exchanger designs, heat exchanger plate spacing (b), and heat exchanger materials into the design space of the optimization problem. However, the preliminary objective was to begin with a comprehensible problem. After understanding the system behavior from this preliminary study, the dimensionality of the optimization problem can then be further increased. A critical parameter that has been discarded in this regard was the plate spacing (b) of the EHX and CHX. The plate spacing of the heat exchanger governs the mass flux of the exhaust and coolant flow streams. However, including the plate spacing in the design space of the problem increases its complexity and, as stated previously, the preliminary objective was to begin with a comprehensible problem.

Some design choices were also not included in the design optimization because the appropriate choice can be made based on a rational judgement. For example, the appropriate candidate for the thermoelectric material and heat exchanger material can

be determined through a straight-forward rational judgement as opposed to including different materials in the design space. This will result in minimizing the complexity of the problem and a computationally inexpensive solution. For example, a comparison of the ZT between the Bi_2Te_3 and QW will show that better TEG systems, size, and efficiency, can be designed and developed using QW material. Likewise, a comparison of the thermal conductivity between copper and carbon steel (AISI1018) will show that the heat exchangers fabricated using copper will minimize the thermal resistance to the heat flow to and from the thermoelectric modules.

Also a comparison between the previously listed design variables for the thermoelectric legs and couples and the design variables investigated in this study shows that the design variables, area of the thermoelectric leg (A_l) and the length of the thermoelectric leg (l_l) are discarded and a new design variable, the aspect ratio of the thermoelectric leg (γ) is introduced. The two independent design variables A_l and l_l have been combined to form a single design variable, γ. This was based on the reasoning that the electrical resistance and thermal conductance of the thermoelectric legs are a function of the aspect ratio of the thermoelectric leg, equations (2.18) and (2.24), rather than the cross-sectional area or length of the thermoelectric legs. Inclusion of both the cross-sectional area or length of the thermoelectric legs into the design space can lead to multiple optimum designs, which might be misleading.

Similarly from the previously listed constraints the following equality constraints were discarded,

$$\begin{bmatrix} L_x\,(\mathrm{EHX}) = L_x\,(\mathrm{CHX}) \\ L_y\,(\mathrm{EHX}) = L_y\,(\mathrm{CHX})\,, \end{bmatrix} \tag{3.10}$$

where the constraint $L_x\,(\mathrm{EHX}) - L_x\,(\mathrm{CHX})$ is the length of EHX parallel to the flow stream must be equal to the length of CHX parallel to the flow stream and the constraint $L_y\,(\mathrm{EHX}) - L_y\,(\mathrm{CHX})$ is the length of EHX normal to the flow stream

must be equal to the length of CHX normal to the flow stream. The exclusion of these two constraints was due to the structure of simulator code design. Instead of creating independent L_x and L_y for each of the EHX and CHX, the simulator code consist of a single L_x and L_y. As discussed in the design of the simulator, section (2.4), the complete TEG system was partitioned into equal sized thermal sections and the energy conserved governing equations of all the thermal sections were solved simultaneously to determine the temperature distribution along the L_x. The simulator code was structured such that the L_x of the EHX and CHX partitions in a single thermal section were equal. Similarly, the L_y of the EHX and CHX partitions in a single thermal section were also equal. Thus not requiring the set of equality constraints listed in equation set (3.10) and minimizing the problem size.

3.6 Optimization: Problem Statement

From the prior discussion, the TPG optimization problem investigated in this study is stated as follows,

$$\begin{aligned} \min_{\vec{x}} \;\; & f(\vec{x}) \\ \text{subject to} \;\; & c(x) \;\leq\; 0 \\ & lb \;\leq\; \vec{x} \;\leq\; ub. \end{aligned} \tag{3.11}$$

$f(\vec{x})$, the function to be minimized is,

$$f(\vec{x}) = -\text{net power}\,(P_{net})\,. \tag{3.12}$$

$c(x)$, the set of inequality constraints are,

$$c(x) = [T_h - c_1]\,, \tag{3.13}$$

where T_h is the hot junction temperature and c_1 is the maximum allowable hot junction temperature. This constraint was applied when using Bi_2Te_3 thermoelectric material. The maximum continuous temperature limit for the Hi-Z HZ20 module is 250 ^oC [38]. lb is the vector of lower limits on the design variables, $\vec{x} = [L_x, L_y, \dot{m}_f, \zeta, \gamma]^T$ is the vector of design variables, and ub is the vector of upper limits on the design variables.

3.7 Optimization: Strategy and Solver

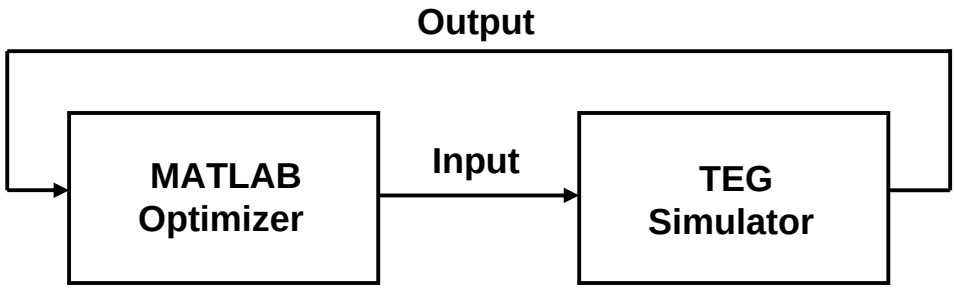

Figure 3.5: TPG optimization strategy

The strategy used for optimizing the previously defined problem is shown in figure (3.5). The strategy was based on a black-box type relationship between the optimizer and the simulator. Though the optimizer was unaware of what goes on inside the simulator, a big advantage of this framework was that the simulator model can change and evolve to incorporate additional elements while the optimizer remains unchanged. In addition, in such a framework the optimizer can be used as a generic

model. MATLAB optimization toolbox was used as the the optimizer. The MATLAB optimization toolbox consists of several solvers and strategies to address various types of optimization issues. The solver specifically used for the TPG optimization is a sequential quadratic programming implementation based on active set strategy or projection method [39].

Using the previously discussed TEG simulator and the optimization strategy, optimization studies were performed. Results showed the existence of multiple optimum designs. Therefore to investigate and resolve the multiple optimum design issues, state space studies were performed on all the design variables in conjunction with the TEG simulator. The methodology used in performing these studies and the resulting response parameters behavior is discussed in the subsequent chapter.

Chapter 4

TPG State Space Studies

The objective of this chapter is to do a preliminary study of the response surfaces of the model to variations of the design variables. This is necessary to ensure that the solution space is fairly smooth without any local minima and the solution is unique. Specifically, the effect of couple density and leg aspect ratio was examined, because in the preliminary attempts, these variables resulted in a non-unique optimal solutions. The chapter begins with an overview of the simulation parameters and the methodology used in this study, followed by a discussion of the results and their physical significance.

4.1 Simulation Parameters

To avoid performing state space studies for each of the cases 1 and 2 and due to the simple system design of case 2, an open loop coolant system and the lack of weight parasitic loss, the simulation parameters from the case 2 were used to perform this particular numerical experiment. As listed in section (3.4), the primary simulation input parameters consisted of,

- Exhaust inlet temperature, ($T_{e,i}$)
- Exhaust mass flow rate, ($\dot{m}_e$)
- Coolant inlet temperature, ($T_{f,i}$).

Furthermore, as discussed in section (3.3) parameters are also required to estimate the various parasitic losses. In the following simulation parameters and their data source used in this study are discussed.

Case 2 data was obtained using a combination of data from the baseline simulation results and the specification sheet for the John Deere Power Tech 6068H Diesel engine for generator set applications [36]. The baseline simulations were performed using a CNG engine model. The engine model was developed using Matlab and Simulink based components from the library of ADVISOR. Since ADVISOR was designed as a vehicle analysis tool, changes were made to the engine model to account for the stationary characteristics of case 2. The data used in case 2 state space studies is listed in table (4.1). The exhaust flow rate and temperature are the mean values for the electrical load varying from 124 to 143 kW and the AC generator efficiency varying from 88 to 92%.

Table 4.1: Case 2 simulation parameters for the state space studies

Variable		Value	Standard Deviation
$\dot{m}_e$	(kg/s)	0.1625	0.0076
$T_{e,i}$	(^oC)	468.54	0.1
$T_{f,i}$	(^oC)	15	-
η_{pcu}	(-)	0.88	-
η_{aa}	(-)	0.88	-

4.2 Methodology

As there were a total of five design variables, $[L_x, L_y, \dot{m}_f, \zeta, \gamma]$, the numerical experiment consists of fixing the three design variables and evaluating responses such as net power, TEG power, etc., as a function of the remainder of the two design variables. This resulted in a total of ten different state space studies corresponding to the five design variables.

Of the several state space studies that have been performed, it has been found that the combination of couple density and thermoelectric leg aspect ratio will result in a multiple optimum designs. In the subsequent sections the results from this particular study and its implication on the optimization problem formulation is discussed.

4.3 State Space Study: ζ Versus γ

Numerical simulations were performed to study the combined effect of couple density (ζ) and thermoelectric leg aspect ratio (γ) on responses such as net power, TEG power, etc. As discussed previously, three design variables were fixed and the variation of the responses such as net power, TEG power, etc., as a function of the remainder of the two variables was studied. In this particular study, L_x, L_y, and $\dot{m}_f$ were the three fixed variables and ζ and γ were the remainder of the variables, whose combined effect on the responses such as net power, TEG power, etc., was analyzed. The range of values for each of the design variables, investigated in this study are listed below,

- $L_x\ (m) = [10^{-1},\ 10^0,\ 10^1]$,
- $L_y\ (m) = [10^{-1},\ 10^0,\ 10^1]$,
- $\dot{m}_f\ \left(\frac{kg}{s}\right) = [0.5,\ 4,\ 12,\ 20]$,
- $\zeta\ \left(\frac{1}{m^2}\right) = [1,\ 2,\ ...,\ 1e10]$, and
- $\gamma\ \left(\frac{1}{m}\right) = [1,\ 2,\ ...,\ 1e10]$.

It should be emphasized that some of the combinations from the above listed design variables though conceptually valid, realizing such designs might not be practically feasible due to material, physical, or other constraints. For example, using a single couple over a system size of about $A_{xy} = 100\ (m^2)$ or packaging 10^8 couples on to an area of about $A_{xy} = 100\ (cm^2)$ might not be practically feasible. However, a wide range of combinations of couple density and leg aspect ratio were studied to verify the existence of any anomalies in the trends of net power, TEG power, etc.

It was observed that the trends for the responses such as net power, TEG power, etc., were similar at various combinations of L_x, L_y, and $\dot{m}_f$. Thus, to further simplify the analysis, discussion of the results is limited to the following combination of fixed variables, $L_x = 1\ (m)$, $L_y = 1\ (m)$, and $\dot{m}_f = 0.5\ (kg/s)$.

4.3.1 Trends of Net Power and TEG Power

Figure (4.1) shows the combined effect of couple density (ζ) and aspect ratio of thermoelectric leg (γ) on the response parameters, net power and TEG power at a fixed system size (L_x and L_y), and coolant mass flow rate ($\dot{m}_f$). The discontinuities in the maximum net power band is a consequence of the discreetly spaced couple density and leg aspect ratio vectors used in the simulations. Finer grain studies were performed to show that this is an artifact of the discretization. From these plots

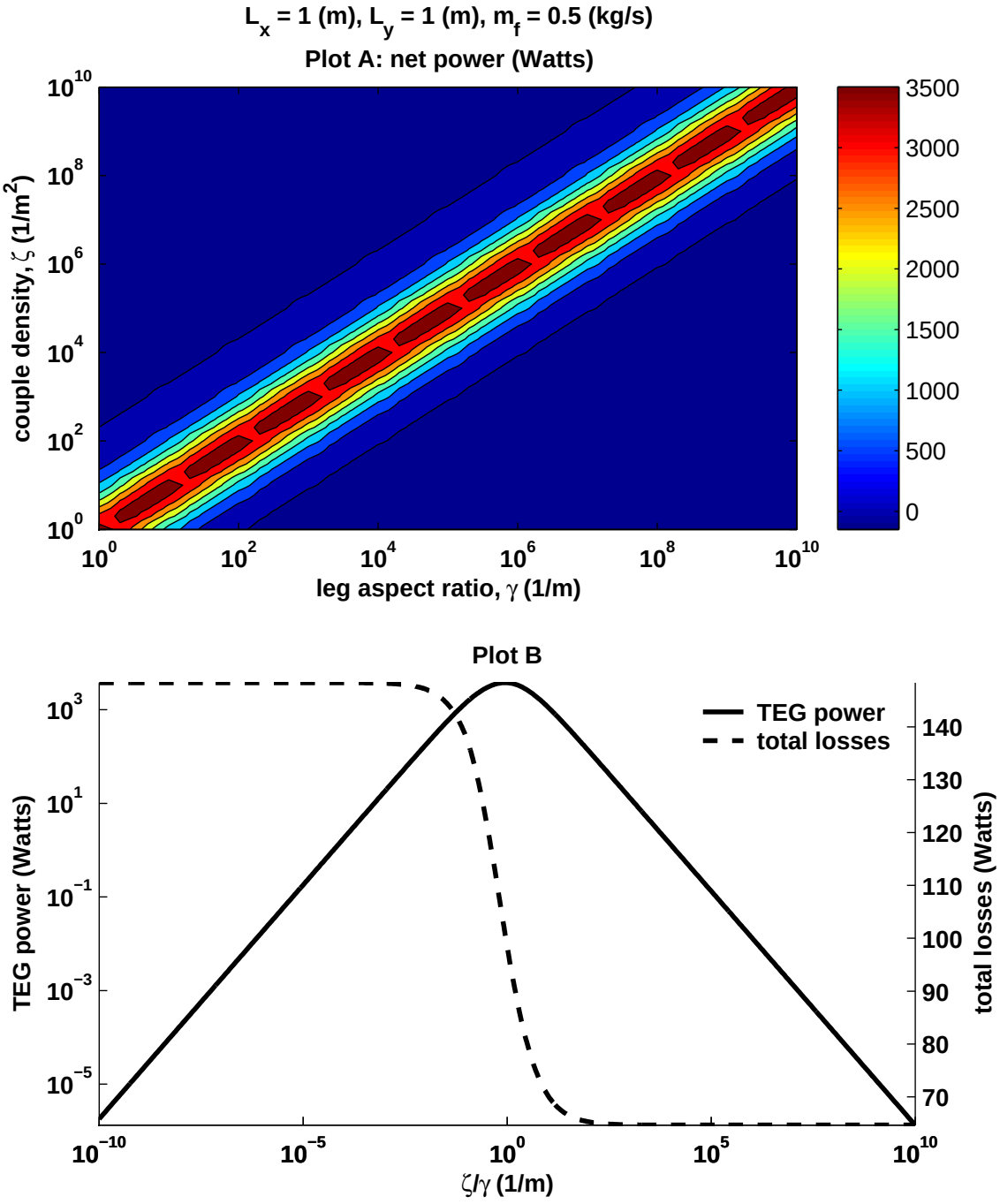

Figure 4.1: Variation of net power and TEG power as a function of couple density and leg aspect ratio

it can be concluded that for a fixed system size, flow conditions, heat exchanger designs, and thermoelectric material, there exists a optimum ratio of couple density to thermoelectric leg aspect ratio $\left(\frac{\zeta}{\gamma}\right)$ at which the bands of maximum net power and TEG power occur. The plots also show that the maximum net power and TEG power bands are independent of both the couple density and leg aspect ratio and rather are only a function of the optimum ratio of couple density to leg aspect ratio. Plot B in figure (4.1) shows that the maximum net power approximately occurs at $\frac{\zeta}{\gamma} = 1\ (1/m)$. The $\frac{\zeta}{\gamma}$ at which the maximum net power occurs is a function of the exhaust and coolant flow conditions, heat exchanger designs, and thermoelectric material.

4.3.2 Functional Dependence of TEG Power on $\frac{\zeta}{\gamma}$

In the following, the previously discussed trend exhibited by the TEG power as a function of the ratio of couple density to leg aspect ratio, is investigated. Using equations (2.22) and (2.25) the power generated by the TEG system, at matched load, is given by,

$$P_g = \left(\frac{1}{4}\right)\left(\frac{V_{oc}^2}{R_g}\right). \tag{4.1}$$

Analogous to equation (2.20), the V_{oc}, the open circuit voltage for the generator is,

$$V_{oc} = \alpha_g \Delta T_g, \tag{4.2}$$

where α_g is the Seebeck coefficient of the generator and ΔT_g is the average junction temperature difference. From equations (4.1) and (4.2) the power generated by the TEG system is,

$$P_g = \left(\frac{1}{4}\right)\left(\frac{\alpha_g^2 \Delta T_g^2}{R_g}\right). \tag{4.3}$$

Equation (4.3) can rearranged as,

$$P_g = \left(\frac{1}{4}\right)\left(\frac{\alpha_g^2}{R_g}\right)\left(\Delta T_g^2\right). \tag{4.4}$$

From equation (4.4), the TEG power is proportional to each of the following terms, $\frac{\alpha_g^2}{R_g}$ and ΔT_g and the average junction temperature difference, ΔT_g, is inversely proportional to the device thermal conductance, K_g. The term $\frac{\alpha_g^2}{R_g}$ for the purpose of discussion would be referred to as the device power factor. Using equations (2.7) and (2.19), the device power factor and the device thermal conductance are given by,

$$\left.\begin{aligned} \text{device power factor} &= A_{xy}\left(\tfrac{\zeta}{\gamma}\right)\left[\tfrac{(\bar{\alpha}_p-\bar{\alpha}_n)^2}{(\bar{\rho}_p+\bar{\rho}_n)}\right] \\ K_g &= A_{xy}\left(\tfrac{\zeta}{\gamma}\right)\left(\bar{k}_n+\bar{k}_p\right) \end{aligned}\right\}. \tag{4.5}$$

Equation set (4.5) shows that each of the device power factor and device thermal conductance are directly proportional to the ratio of couple density to aspect ratio of the legs. However, the device power factor and the device thermal conductance are two competing effects. Therefore, the couple density and leg aspect ratio do not matter individually and only their ratio determines the maximum net and TEG power.

4.3.3 Existence of an Optimum $\frac{\zeta}{\gamma}$: Analytical Solution

In the previous section numerical studies were performed to investigate the existence of an optimum ratio of couple density to leg aspect ration, ψ, at which the maximum TEG power occurs. However, the studies were explicitly based on a fixed set of flow conditions, heat exchanger designs, and thermoelectric material. Therefore, in this section it is shown analytically that an optimum ratio of couple density to leg aspect ratio exists independent of flow conditions, heat exchanger designs, and thermoelectric

material.

The analysis was performed under assumptions similar to that of the TEG simulator model. To simplify the analysis the following additional assumptions were also made, (1) the thermoelectric material properties do not vary as a function of temperature and (2) the bulk temperature of the exhaust and coolant are uniform within the EHX and CHX respectively, this corresponds to the case where the space for the device is highly limited and only a small portion of the exhaust power can be extracted.

Figure (4.2) shows a thermal circuit model of a TEG system sandwiched between

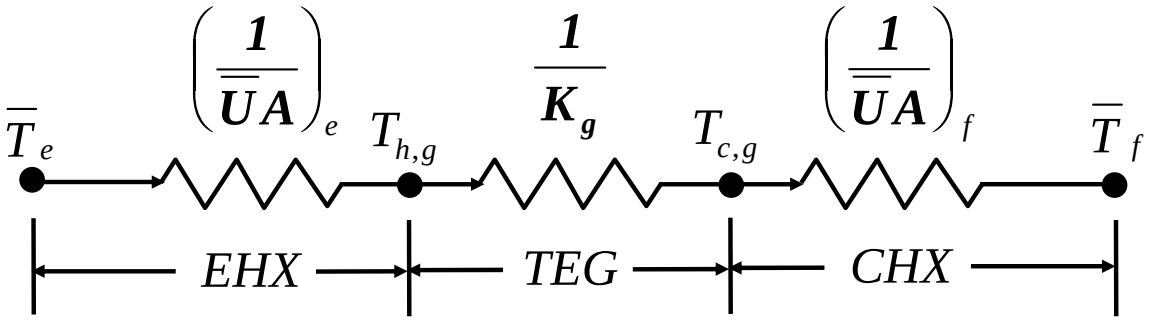

Figure 4.2: Thermal circuit model of a TEG system

an EHX and a CHX, where the $\overline{T}_e$ is the average bulk temperature of the exhaust, $\left(\frac{1}{\overline{U}A}\right)_e$ is the total thermal resistance on the exhaust side, $\frac{1}{K_g}$ is thermoelectric device thermal resistance, and $\overline{T}_f$ and $\left(\frac{1}{\overline{U}A}\right)_f$ have definitions similar to that of the $\overline{T}_e$ and $\left(\frac{1}{\overline{U}A}\right)_e$ but for the coolant side. $\overline{U}$ is the average overall heat transfer coefficient and A is the heat transfer area.

As the limit of the thermoelectric device efficiency, η_g, tends to zero, energy from the exhaust transferred through the thermoelectric device is completely rejected to the coolant and under such a scenario, the junction temperature difference across the thermoelectric device is given by,

$$\Delta T_g = \frac{\frac{1}{K_g}}{\left(\frac{1}{\overline{U}A}\right)_e + \frac{1}{K_g} + \left(\frac{1}{\overline{U}A}\right)_f} \left(\overline{T}_e - \overline{T}_f\right), \tag{4.6}$$

and from equations (4.4), (4.5), and (4.6) the TEG power as a function of $\overline{T}_e$ and $\overline{T}_f$ is given by,

$$P_g = \frac{\left(\frac{1}{4}\right) A_{xy} \left(\frac{\zeta}{\gamma}\right) \left[\frac{(\bar{\alpha}_p - \bar{\alpha}_n)^2}{(\bar{\rho}_p + \bar{\rho}_n)}\right]}{\left[A_{xy} \left(\frac{\zeta}{\gamma}\right) \left(\bar{k}_n + \bar{k}_p\right) \left[\left(\frac{1}{\overline{U}A}\right)_e + \left(\frac{1}{\overline{U}A}\right)_f\right] + 1\right]^2} \left(\overline{T}_e - \overline{T}_f\right)^2. \tag{4.7}$$

At a fixed system size (L_x and L_y) and at constant thermoelectric material properties, maximizing TEG power, equation (4.7), with respect to $\frac{\zeta}{\gamma}$, $\left(\frac{\partial P_g}{\partial\left(\frac{\zeta}{\gamma}\right)} = 0\right)$, yields,

$$\frac{\zeta}{\gamma} = \frac{1}{A_{xy} \left(\bar{k}_n + \bar{k}_p\right) \left[\left(\frac{1}{\overline{U}A}\right)_e + \left(\frac{1}{\overline{U}A}\right)_f\right]}. \tag{4.8}$$

Equation (4.8) shows that at matched load conditions there exists an optimum ratio of couple density to leg aspect ratio, $\frac{\zeta}{\gamma}$, at which the maximum TEG power occurs. Furthermore, the maximum TEG power is independent of the couple density, ζ, and leg aspect ratio, γ, and instead can be attained as long as the ratio of couple density to leg aspect ratio is maintained at the optimum. The magnitude of the optimum ratio of couple density to leg aspect ratio can be approximated by equation (4.8) and the error of this approximation increases proportional to the device efficiency and is zero at open circuit.

Combining equations (4.5) and (4.8), the thermal conductance of the device is given by,

$$K_g = \frac{1}{\left(\frac{1}{\overline{U}A}\right)_e + \left(\frac{1}{\overline{U}A}\right)_f}. \tag{4.9}$$

Equation (4.9) shows that the maximum TEG power occurs when the combined thermal resistance of the exhaust and coolant sides is equal to the thermal resistance of the thermoelectric device. This particular observation was also reported by Henderson [40] and Stevens [41].

4.4 Redefined TPG Optimization

In the prior section it was observed numerically and analytically the existence of an optimum ratio of couple density to leg aspect ratio at which the maximum TEG power occurs. As a result, encompassing the variables couple density, ζ, and leg aspect ratio, γ, simultaneously within the design variables vector will result in multiple optimum designs and might possibly lead to unintended optimum design solutions. Therefore, to address this issue the TPG optimization problem statement is modified and redefined.

The strategy is to fix either of the couple density or leg aspect ratio and retaining the other as a design variable. This will result in a unique optimum couple density or leg aspect ratio. In the current work couple density is the fixed variable and leg aspect ratio is the design variable. The couple density was fixed at 1.28×10^4 ($\frac{1}{m^2}$). This value is based on the approximate couple density of the HZ20 module [38].

4.5 State Space Study to Establish Uniqueness

Additional numerical studies are performed to determine the response of net power, as a function of the remainder of the design variables, L_x, L_y, and $\dot{m}_f$. The objective of these studies is to verify whether the objective function, net power, is smooth and the solution obtained would be unique.

Figure (4.3) shows the contours of net power as a function of L_x and L_y at a fixed

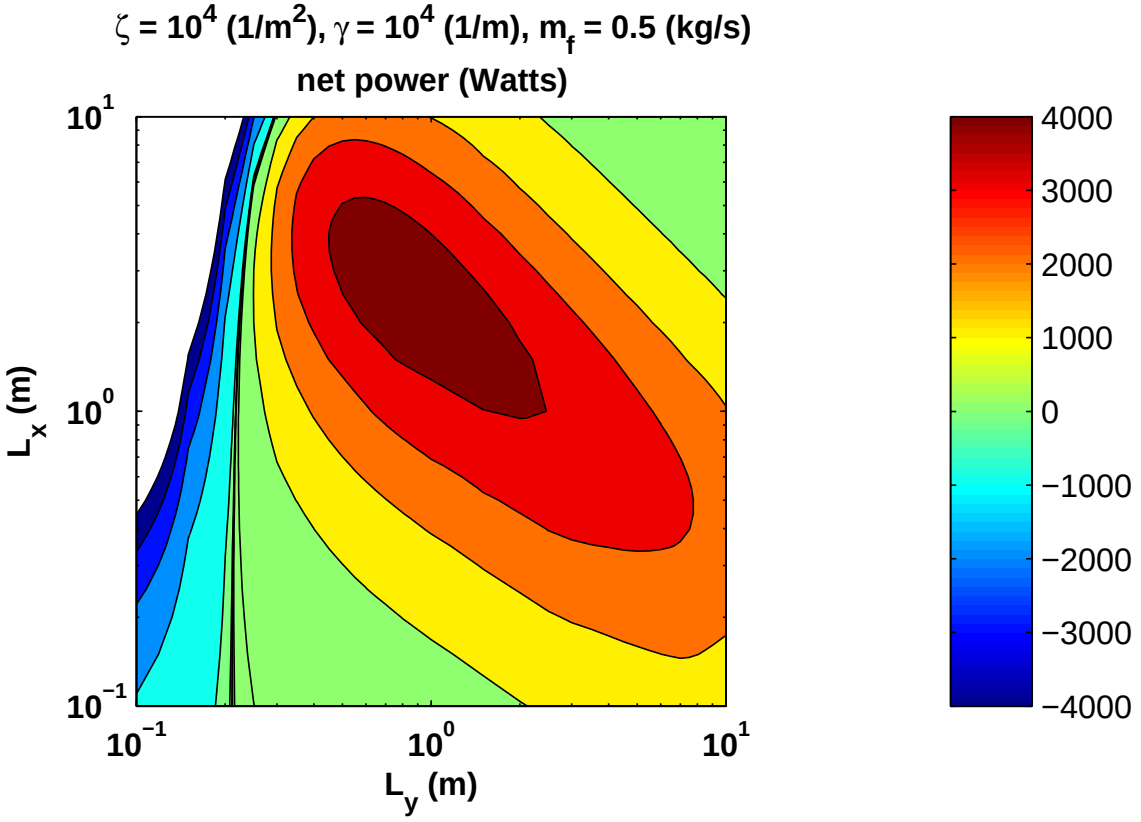

Figure 4.3: Contours of net power as a function of L_x and L_y

couple density, $\zeta = 10^4 \ \left(\frac{1}{m^2}\right)$, leg aspect ratio, $\gamma = 10^4 \ \left(\frac{1}{m}\right)$, and coolant mass flow rate, $\dot{m}_f = 0.5 \ \left(\frac{kg}{s}\right)$. As shown in the figure there is a unique maximum net power. Figure (4.3), also shows that the objective function, net power, is relatively smooth in

the domain space of L_x and L_y. Similarly, numerical studies were also performed to study the variation of the net power as a function of the design variables, L_x and $\dot{m}_f$, at a fixed $L_y = 1\ (m)$, couple density, $\zeta = 10^4\ \left(\frac{1}{m^2}\right)$, and leg aspect ratio, $\gamma = 10^4\ \left(\frac{1}{m}\right)$. As shown in figure (4.4), the contours shows that there is a unique maximum net

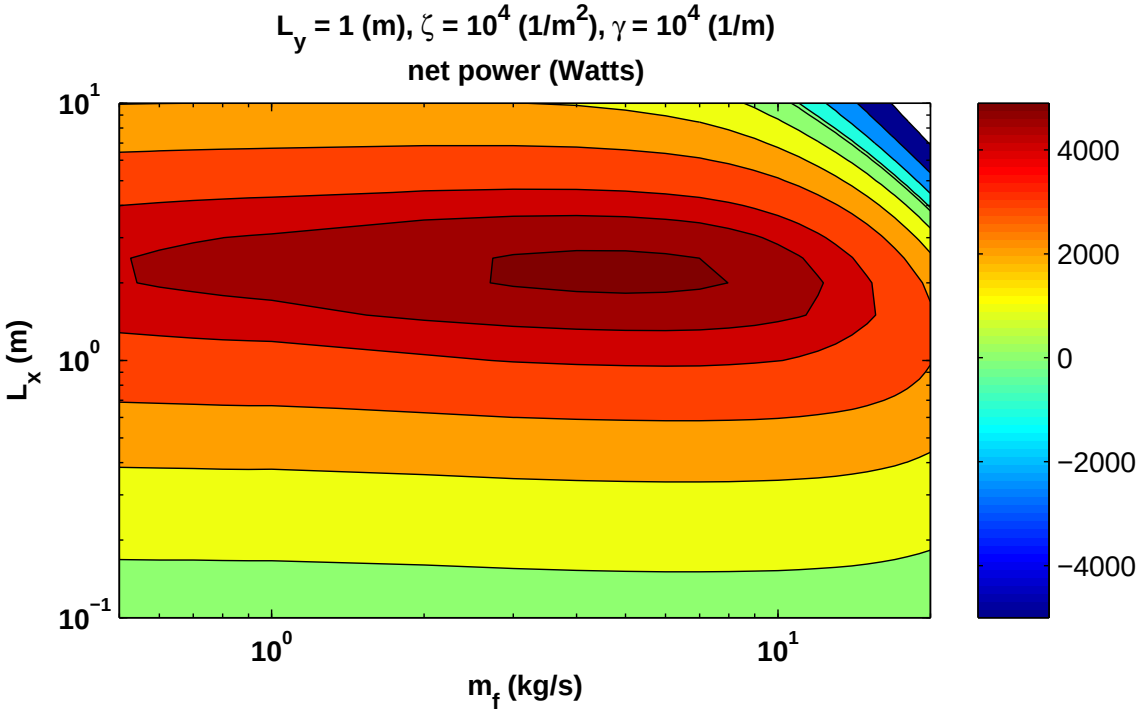

Figure 4.4: Contours of net power as a function of L_x and $\dot{m}_f$

power in the domain space of L_x and $\dot{m}_f$. Likewise the uniqueness of maximum net power was observed for the remainder of the design variables combinations, except for the combination of couple density, ζ, and leg aspect ratio, γ.

Based on the previously discussed state space studies and with the modified vector of design variables optimization studies were performed for Case 1. The studies were performed using either of the QW or Bi_2Te_3 material. In the subsequent chapter the results from these studies are discussed.

Chapter 5

Optimization Results

In this chapter optimization results of Case 1, a sports-utility vehicle, are reported and discussed. The objective of this chapter is to determine an optimum design and to understand how that design depends on the inputs into the model, such as flow conditions, material properties, and size limitations, etc. Each design variable is investigated to understand what are the governing processes that determine the optimal point. We then investigate how that optimal point changes for different geometries of the TEG. This is important because in many mobile applications there are significant space constraints. All of these analysis are performed at 70 (mph) vehicle speed using QW-TEG. The variation of the optimal design variables and the performance with vehicle speed and thermoelectric material is investigated and the change in performance when using a single design for all vehicle speed is assessed. In the final section studies are performed to assess the change in performance and the optimum design between the mobile and stationary applications.

5.1 Simulation and Optimization Parameters

The sports-utility vehicle system described in section(3.1) is used for the optimization studies. The flow conditions and other vehicle data are obtained using a combination of results from the testing performed at Delphi [11], ADVISOR baseline simulations, and data supplied by GMC. ADVISOR is a MATLAB and Simulink-based vehicle simulator developed at NREL [2]. The baseline simulations were performed using an altered vehicle system model from the library of the ADVISOR. Changes were made such that the parameters, exhaust inlet temperature, $T_{e,i}$, exhaust mass flow rate, $\dot{m}_e$, and coolant inlet temperature, $T_{f,i}$, predicted by the altered model were representative of the vehicle used in the testing performed at Delphi. The data used in Case 1 optimization studies is listed in table (5.1).

Table 5.1: Case 1 simulation parameters for the optimization studies

v (mph)	$\dot{m}_e$ (kg/s)	$T_{e,i}$ (^oC)	$T_{f,i}$ (^oC)	η_{pcu}	η_{ag}	η_D	μ_R
30	0.0156	467.23	88	0.88	0.5	0.89	0.012
50	0.0274	575.46					
70	0.05	672					

The optimization is performed at various combinations of L_x and L_y and at a fixed couple density, ζ, as listed below,

- $L_x = [0.2,\ 0.3,\ ...,\ 1]\ (m)$
- $L_y = [0.2,\ 0.3,\ ...,\ 1]\ (m)$
- Couple density, $\zeta = 1.28 \times 10^4\ \left(\frac{1}{m^2}\right)$.

The range of L_x and L_y is limited to less than 1 (m) due to the limited space under the vehicle body for the installation of TEG. In fact any designs that might result in

L_x or L_y greater than 75 (cm) might itself be constrained with respect to the space available under the vehicle body. For example, the size of the prototype TEG used in the vehicle testing is about L_x=34.3 (cm) and L_y= 19 (cm).

As discussed previously, the couple density and leg aspect ratio do not matter individually and only their ratio determines the maximum TEG power and the inclusion of couple density and leg aspect ratio together as design variables would result in multiple optimum designs. Accordingly, in this work the couple density is the fixed variable and the leg aspect ratio is the design variable. As listed, the couple density is fixed at 1.28×10^4 $(\frac{1}{m^2})$ and this value is based on the approximate couple density of the HZ20 module [38].

The design variables investigated in this study have the following bounds,

- coolant mass flow rate, $\dot{m}_f$
  - lower bound 0.01 $\left(\frac{kg}{s}\right)$
  - upper bound 3 $\left(\frac{kg}{s}\right)$
- leg aspect ratio, γ
  - lower bound 100 $\left(\frac{1}{m}\right)$
  - upper bound 10^{10} $\left(\frac{1}{m}\right)$.

The bounds on the coolant mass flow rate are established based on the coolant system data of the test vehicle supplied by General Motors [11]. The upper bound on the coolant mass flow rate is the total coolant flow rate through the engine under fully open thermostat condition and at maximum engine loading.

5.2 Results of QW-TEG at 70 (mph) Vehicle Speed

In the following results of QW-TEG at 70 (mph) vehicle speed are investigated to determine what are the main processes that determine the optimal values of each variable and the variation of the optimum point with system size. Specifically the effect of system size on the net power, optimum coolant mass flow rate, and optimum leg aspect ratio.

5.2.1 Effect of System Size (A_{xy})

In the following the effect of system size on the net power is discussed. Figure (5.1) shows the variation of net power at various combinations of L_x and L_y. Also, the

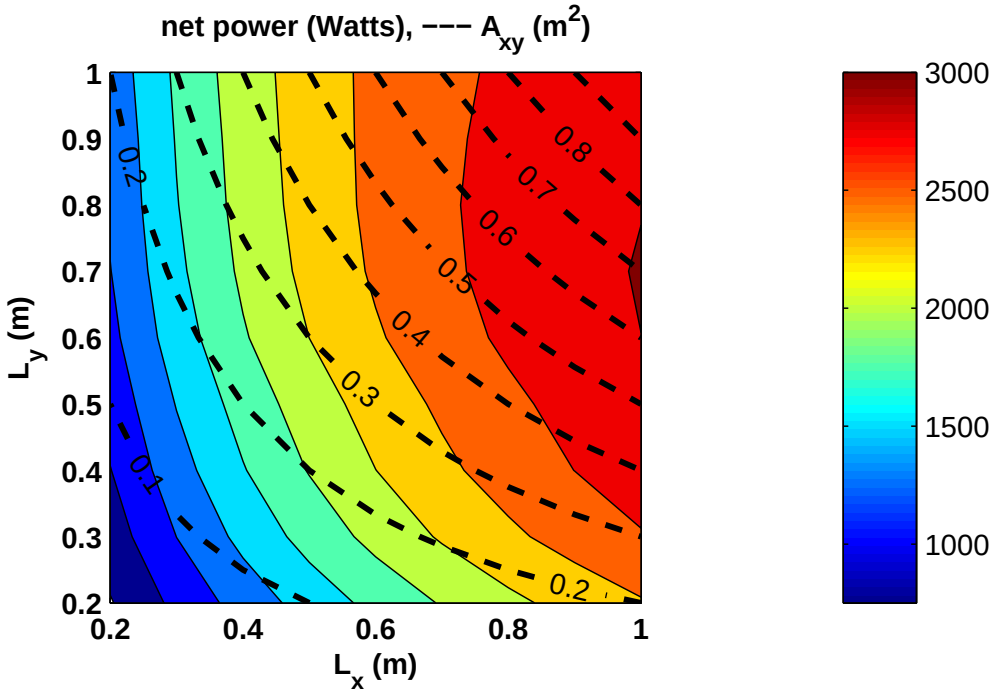

Figure 5.1: Contours of net power using QW-TEG at 70 (mph) vehicle speed

contours of constant A_{xy} are overlaid on to the contours of net power. The plot shows

that the maximum net power is to the right of L_x=1 (m). For mobile applications the optimum system size will often be larger than one can fit into the system.

To understand what determines the optimum system size, an optimization is performed where the Axy is varied while optimizing Lx/Ly, the mass flow rate of the coolant, and the leg aspect ratio. The optimization is performed at 70 (mph) flow conditions using QW-TEG. The variation of net power, TEG power at the shaft, and

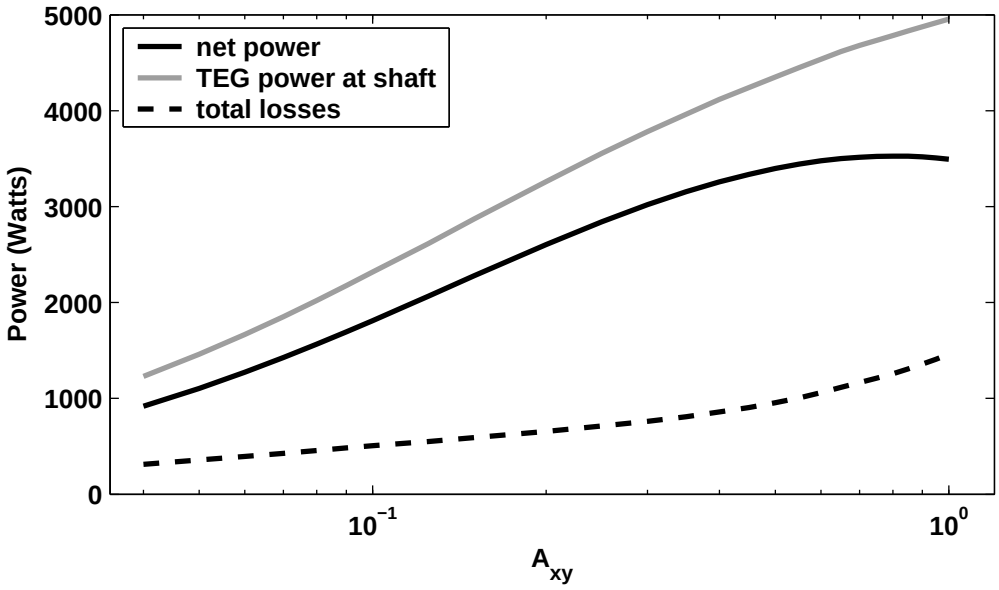

Figure 5.2: Net power, TEG power, and total losses as a function of A_{xy} ratio

the total losses as a function of A_{xy} are shown in the figure (5.2) and the variation of weight parasitic loss, ΔP_D, coolant pumping power, ΔP_P, and blow down work, ΔP_B, are shown in the figure (5.3). The TEG power is converted to its corresponding shaft power as shown in equation (3.1). As shown in the figure (5.2), the net power increases proportional to the A_{xy} and there is an optimum A_{xy} at which the maximum net power occurs. The maximum net power of 3527 $(Watts)$ occurs at A_{xy}=0.8 (m^2) and the optimum $\frac{L_x}{L_y}$ ratio at this A_{xy} is 13.

The TEG power increases proportional to the A_{xy} and on the contrary the total

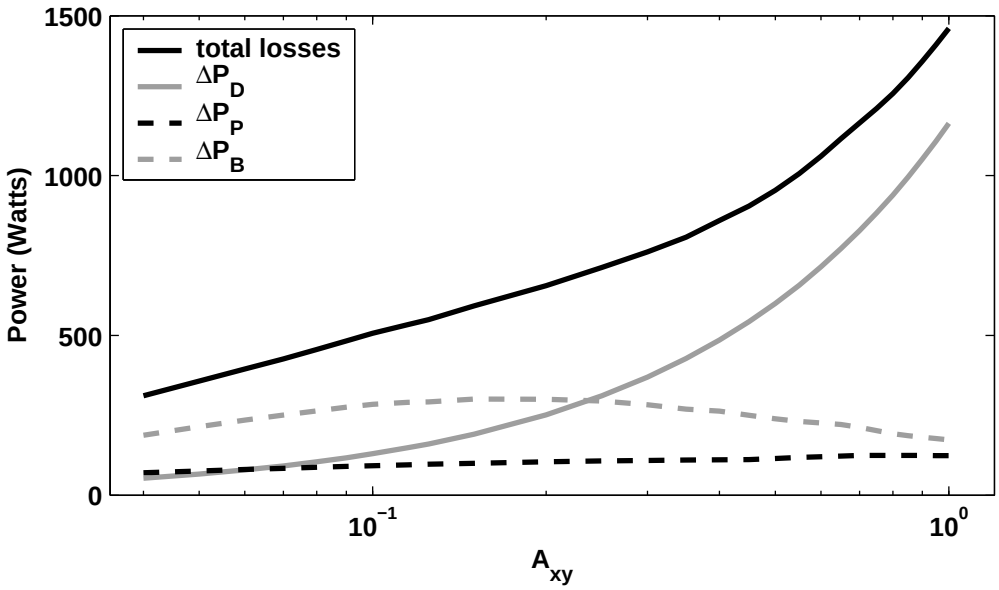

Figure 5.3: Parasitic losses as a function of A_{xy} ratio

parasitic losses also increases proportional to the A_{xy}. These two competing effects resulted in an optimum A_{xy} at which the maximum net power occurs. The increase in the parasitic losses proportional to the A_{xy} is predominantly due to the weight parasitic loss, as shown in figure (5.3). For the system shown in the figure (5.2), the ratio of weight parasitic loss to the total losses varies from 30 % at lower A_{xy} to as high as 85 % at higher A_{xy}.

5.2.2 Effect of $\frac{L_x}{L_y}$ Ratio

Likewise optimization studies are performed to determine the effect of $\frac{L_x}{L_y}$ ratio on the net power. The strategy is to perform the optimization at a fixed A_{xy} and $\frac{L_x}{L_y}$ ratios to determine the optimum coolant mass flow rate and leg aspect ratio. A fixed A_{xy} of 0.2 (m^2) is selected for this analysis. The optimization is performed at various $\frac{L_x}{L_y}$ ratios ranging from 0.4 to 20. The coolant mass flow rate and the leg aspect ratio are optimized at each of the $\frac{L_x}{L_y}$ ratio. The results from this study are shown in the

figures (5.4) and (5.5). The variation of net power, TEG power at the shaft, and the

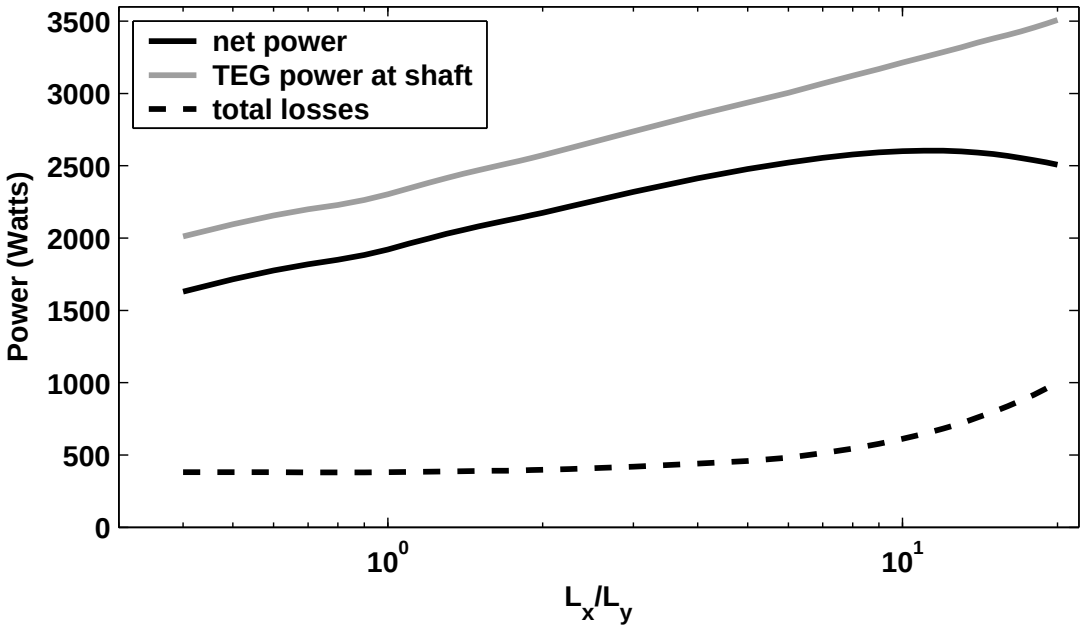

Figure 5.4: Net power, TEG power, and total losses as a function of $\frac{L_x}{L_y}$ ratio

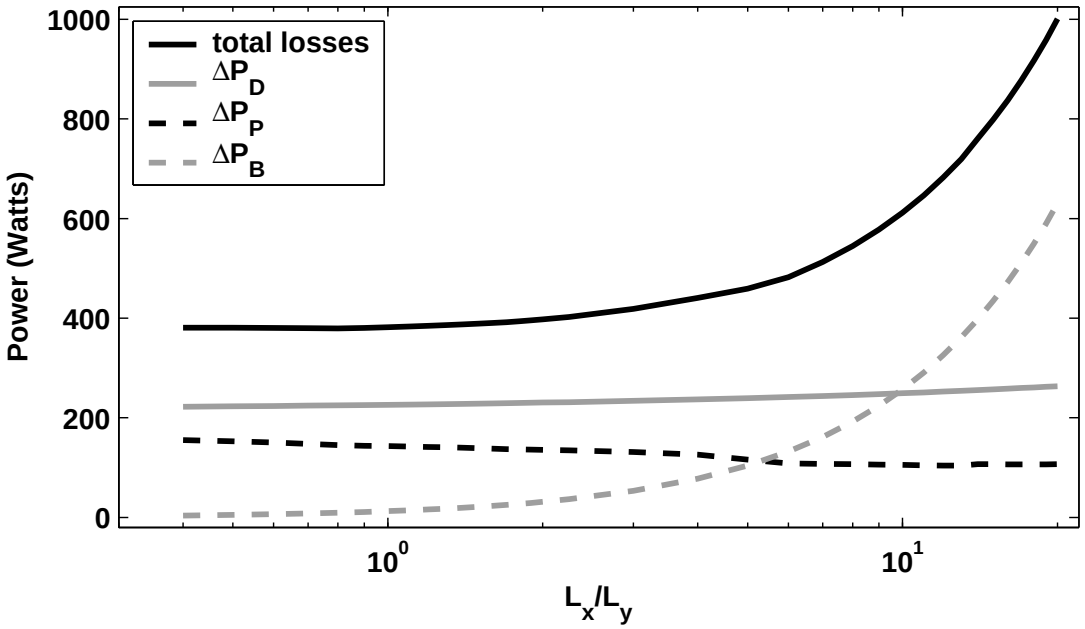

Figure 5.5: Parasitic losses as a function of $\frac{L_x}{L_y}$ ratio

total losses as a function of $\frac{L_x}{L_y}$ ratio are shown in the figure (5.4) and the variation of weight parasitic loss, ΔP_D, coolant pumping power, ΔP_P, and blow down work, ΔP_B, are shown in the figure (5.5). The TEG power is converted to its corresponding shaft power as shown in equation (3.1). From the results shown it can be observed that at a fixed A_{xy} the net power increases proportional to the $\frac{L_x}{L_y}$ ratio and there exists an optimum $\frac{L_x}{L_y}$ ratio at which the maximum net power occurs.

As the exhaust mass flow rate is a fixed quantity, at a fixed A_{xy} the increase in $\frac{L_x}{L_y}$ ratio increases the exhaust mass flow rate per unit cross-sectional area and consequently increases the heat transfer, hot junction temperature, and the TEG power. In contrast, the higher exhaust mass flow rate per unit cross-sectional area also flows through a longer flow channel length resulting in an increase of back pressure and blow down work. These two competing effects, the TEG power and the blow down work, will result in an optimum $\frac{L_x}{L_y}$ ratio at which the maximum net power occurs. The weight parasitic loss is only a function of A_{xy} and is independent of the $\frac{L_x}{L_y}$ ratio. The variations in the coolant parasitic loss are less significant primarily due to the fact that the exhaust mass flow rate is a fixed quantity and the coolant mass flow rate is a design variable.

5.2.3 Effect of Coolant Mass Flow Rate

In the following, the results of the optimum coolant mass flow rate for the spatially constrained system at 70 (mph) vehicle speed and using a QW-TEG are discussed. The results of optimum coolant mass flow rate discussed in this section correspond to the net power results shown in the figure (5.1).

Optimization studies are performed to determine the effect of coolant mass flow rate on the net power. The strategy is to perform the optimization at a fixed A_{xy}. $\frac{L_x}{L_y}$ ratio, and lag aspect ratio to determine the variation of net power and other response

parameters as a function of coolant mass flow rate. The fixed variable used in this analysis are $A_{xy} = 0.8\,(m^2)$, $\frac{L_x}{L_y} = 1.25$, and leg aspect ratio, $\gamma = 30814\ \left(\frac{1}{m}\right)$. The results from this study are shown in the figures (5.6) and (5.7). The variation of

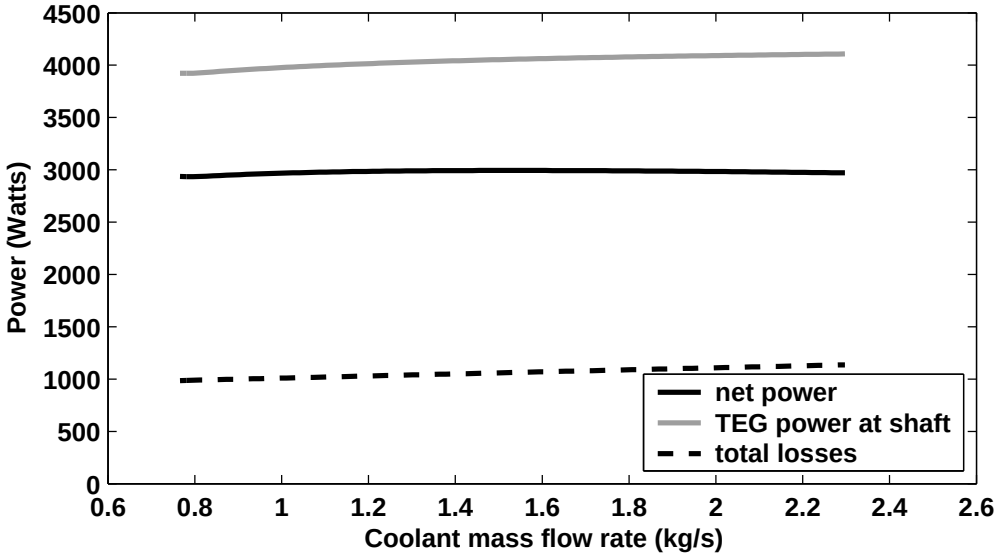

Figure 5.6: Net power, TEG power, and total losses as a function of coolant mass flow rate

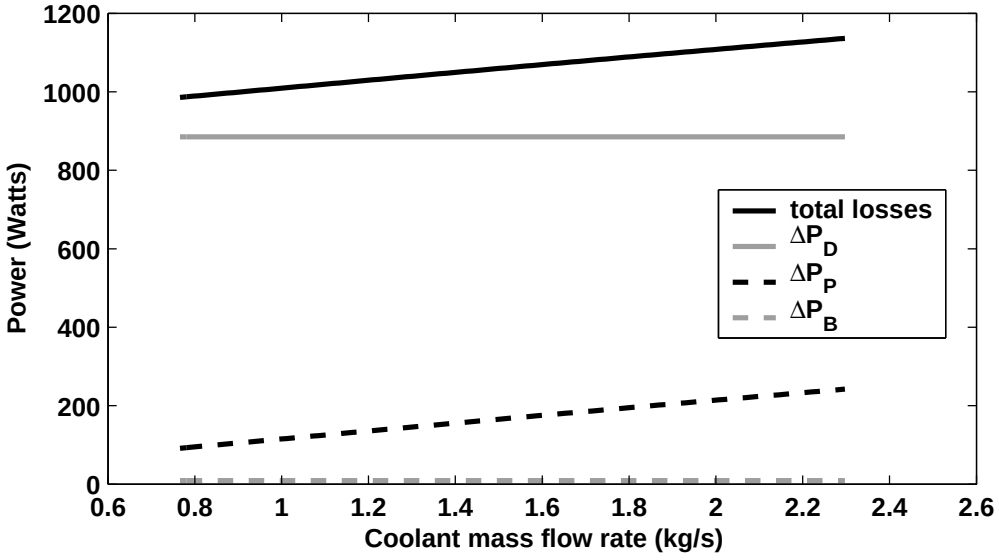

Figure 5.7: Parasitic losses as a function of coolant mass flow rate

net power, TEG power at the shaft, and the total losses as a function of coolant mass flow rate are shown in the figure (5.6) and the variation of weight parasitic loss, ΔP_D, coolant pumping power, ΔP_P, and blow down work, ΔP_B, are shown in the figure (5.7). The TEG power is converted to its corresponding shaft power as shown in equation (3.1). From the results shown it can be observed that the TEG power and parasitic coolant pumping power increases proportional to the coolant mass flow rate. Therefore, there is an optimum coolant mass flow at which the maximum net power occurs. Furthermore, the variation of the coolant mass flow rate do not effect either the blow down work or the weight parasitic loss. The increase of the coolant mass flow rate increases the coolant flow rate per unit area and consequently the heat transfer coefficient and the TEG power and equation (3.5) shows that the pumping power is proportional to the cube of the coolant volumetric flow rate.

Figure (5.8) shows the variation of optimum coolant mass flow rate at various combinations of L_x and L_y. From the plot shown in the figure (5.8), the optimum coolant mass flow is a function of both the A_{xy} and the $\frac{L_x}{L_y}$ ratio and ranges from a value 0.8 $\frac{kg}{s}$ to 1.6 $\frac{kg}{s}$. The heat transfer area increases proportional to the A_{xy} and therefore exhaust energy extracted increases proportional to the A_{xy}. Consequently, the heat rejected to the coolant also increases, requiring a higher coolant mass flow rate to maintain the cold side junction temperatures. Furthermore, figure (5.8) shows that the optimum coolant mass flow rate at a fixed A_{xy} decreases with increasing Lx/Ly ratio. This is because decreasing Lx/Ly causes an increase in flow rate per unit area increasing the heat transfer coefficients and thus requiring less total mass flow rate to maintain the cold junction temperatures.

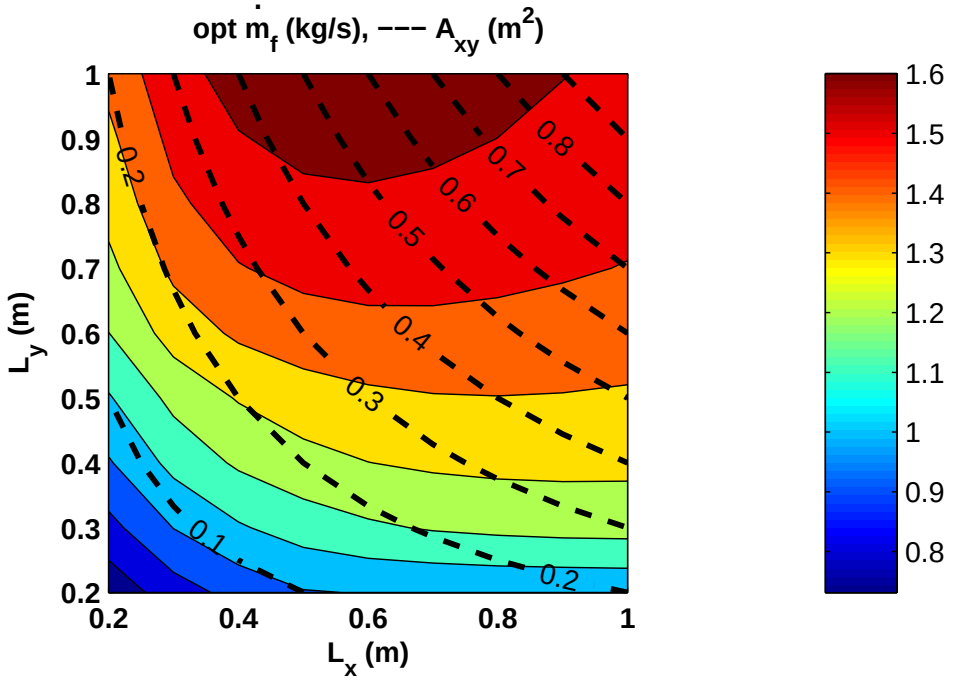

Figure 5.8: Contours of optimal coolant mass flow rate using QW-TEG at 70 (mph) vehicle speed

5.2.4 Effect of Leg Aspect Ratio

In the following, the results of the optimum leg aspect ratio for the spatially constrained system at 70 (mph) vehicle speed and using a QW-TEG are discussed. The results of optimum leg aspect ratio discussed in this section correspond to the net power results shown in the figure (5.1).

Optimization studies are performed to determine the effect of leg aspect ratio on the net power. The strategy is to perform the optimization at a fixed A_{xy}. $\frac{L_x}{L_y}$ ratio, and coolant mass flow rate to determine the variation of net power and other response parameters as a function of leg aspect ratio. The fixed variable used in this analysis are $A_{xy} = 0.8\,(m^2)$, $\frac{L_x}{L_y} = 1.25$, and coolant mass flow rate, $\dot{m}_f = 1.5\ \left(\frac{kg}{s}\right)$. The results from this study are shown in the figures (5.9) and (5.10). The variation of net power,

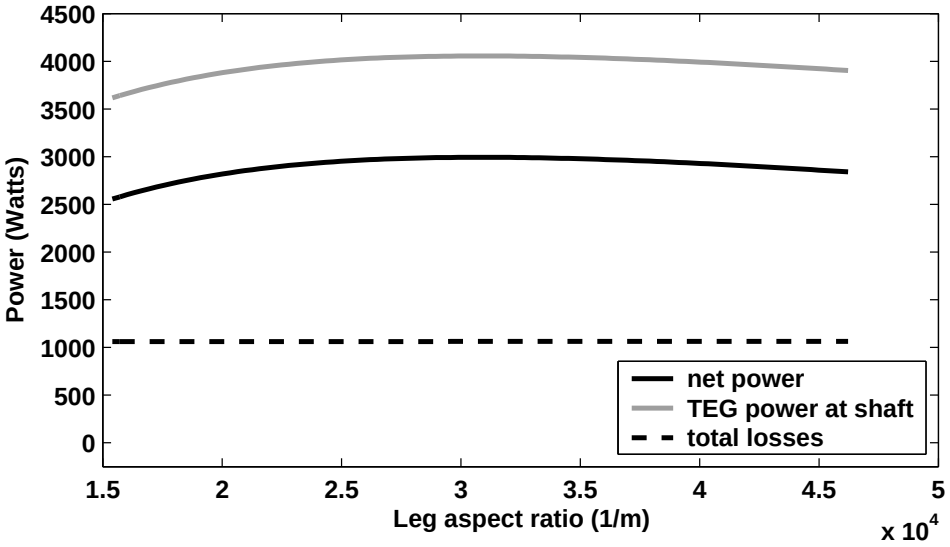

Figure 5.9: Net power, TEG power, and total losses as a function of leg aspect ratio

TEG power at the shaft, and the total losses as a function of coolant mass flow rate are shown in the figure (5.6) and the variation of weight parasitic loss, ΔP_D, coolant pumping power, ΔP_P, and blow down work, ΔP_B, are shown in the figure (5.7). The TEG power is converted to its corresponding shaft power as shown in equation (3.1).

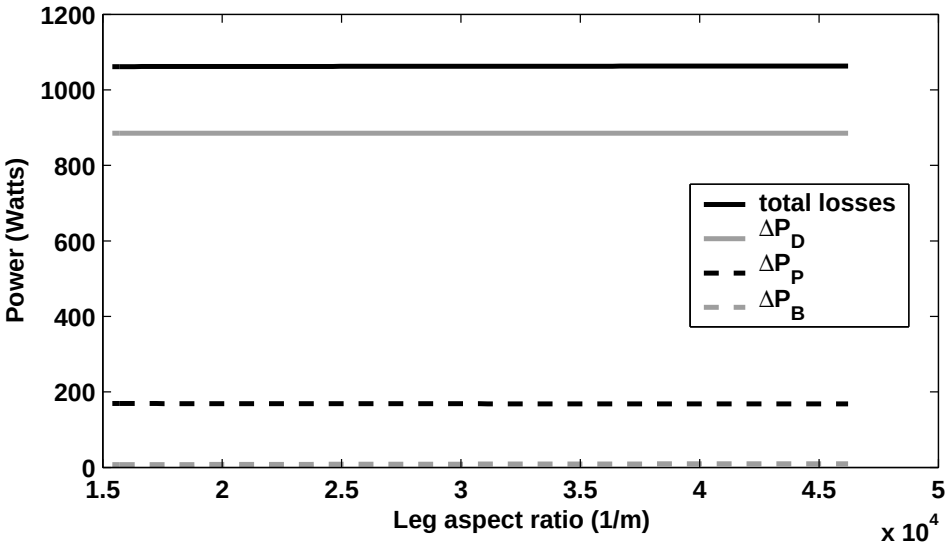

Figure 5.10: Parasitic lossses as a function of leg aspect ratio

From the results shown it can be observed that the there is an optimum leg aspect ratio at which the maximum TEG power occurs. In contrast the total parasitic losses are independent of the leg aspect ratio. This is clearly evident in figure (5.7), where the losses, coolant pumping power, blow down work, and the weight parasitic loss are independent of the leg aspect ratio. As the net power is defined as the difference between the TEG power and the parasitic losses, the maximum net power also occurs at the same optimum leg aspect ratio at which the maximum TEG power occurs. Also, equation (4.8) shows that there is an optimum ratio of couple density to leg aspect ratio at which the maximum TEG power occurs and as the couple density is a fixed quantity there is an optimum leg aspect ratio at which the maximum TEG power occurs.

Figure (5.11) shows the variation of optimum leg aspect ratio at various combinations of L_x and L_y. From the plot shown in the figure (5.11), the optimum leg aspect ratio approximately increases proportional to the A_{xy}. It has been established from equation (4.9), that the maximum TEG power occurs when the combined

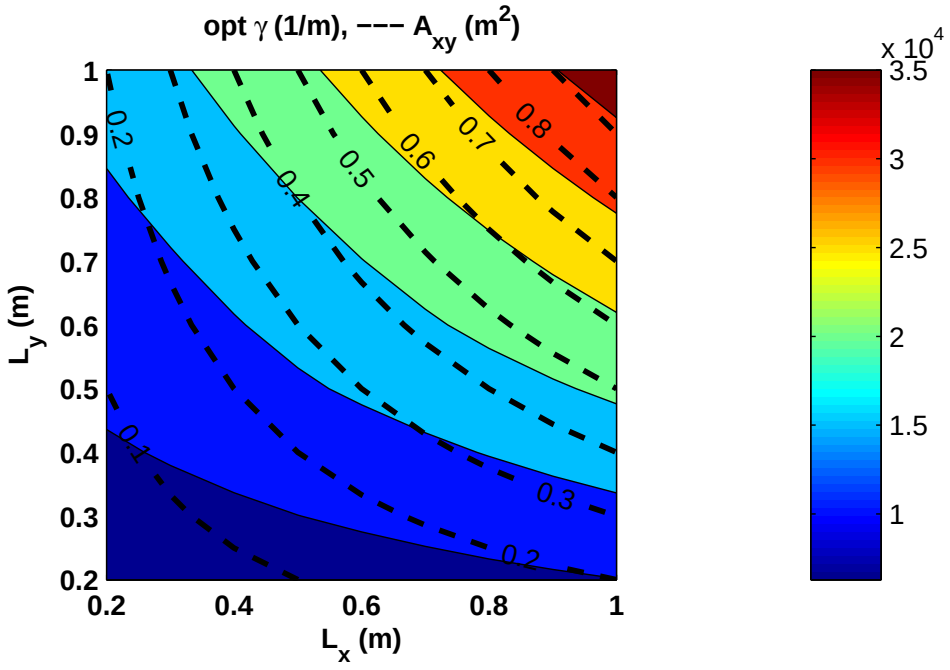

Figure 5.11: Contours of optimal leg aspect ratio using QW-TEG at 70 (mph) vehicle speed

thermal resistance of the exhaust and coolant sides is equal to the thermal resistance of the thermoelectric device. At a fixed $\frac{L_x}{L_y}$ ratio the heat transfer coefficient on the exhaust side decreases proportional to A_{xy} due to the decrease of exhaust mass flow rate per unit area. As a result, the combined thermal resistance of the heat exchanger increases proportional to the A_{xy}. Therefore, from equation (4.9), to maximize the TEG power the thermal resistance of the thermoelectric device must increase which is accomplished by increasing the leg aspect ratio as shown in equation (2.7).

5.3 Effect of Vehicle Speed and Thermoelectric Material

In the following the effect of vehicle speed and thermoelectric material on the net power and the optimum design is investigated. The spatial constraints are such that both the L_x and L_y are constrained to be less than 1 (m). Table (5.2) lists the maximum net power and the corresponding optimum design at each of the 30, 50, and 70 (mph) vehicle speeds using either of the QW or Bi_2Te_3-TEG.

Table 5.2: Effect of vehicle speed and thermoelectric material on net power, system size, and optimum design

vehicle speed (mph)	net power (W)	TEG power at shaft (W)	ΔP_P (W)	ΔP_B (W)	ΔP_D (W)	A_{xy} (m^2)	opt $\dot{m}_f$ $\left(\frac{kg}{s}\right)$	opt γ $\left(\frac{1}{m}\right)$
QW-TEG								
30	393	554	11	1.4	148.7	0.3	0.13	3.75×10^4
50	1153	1549	66.5	4.9	324.7	0.4	0.78	2.83×10^4
70	3015	3968	164.9	11.2	777.5	0.7	1.5	2.75×10^4
Bi_2Te_3-TEG								
30	150	247	33.6	1.5	61.5	0.12	0.48	207
50	354	563	79.5	9.7	119.7	0.14	0.95	101
70	744	1159	156	67.2	191.5	0.16	1.4	54

5.3.1 Net Power

A comparison of net power between different vehicle speeds using either of the QW or Bi_2Te_3-TEG shows that the net power increases proportional to the vehicle speed. The increase of TEG power with vehicle speed is due to the increase of both the exhaust inlet temperature and exhaust mass flow rate. Furthermore at each of the vehicle speed, the A_{xy}, the coolant mass flow rate, and the leg aspect ratio are optimized

to maximize the net power. The significant difference in TEG power between the QW and Bi_2Te_3 is due to the high ZT of the QW material compared to the Bi_2Te_3 material. As shown in the figure (2.10), the ZT of the QW material is higher than the Bi_2Te_3 material by a factor of 1.4 to 2.

A comparison of the A_{xy} at which the maximum net power occurs shows that the A_{xy} increases proportional to the vehicle speed using either of the QW or Bi_2Te_3-TEG. The exhaust mass flow rate and exhaust inlet temperature increases proportional to the vehicle speed resulting in the increase of exhaust energy and consequently the TEG power. The higher TEG power allows higher weight parasitic losses to be supported thus the optimal area, A_{xy}, increases. Furthermore, the rate of increase of A_{xy} with respect to the vehicle speed is higher for the QW compared to the Bi_2Te_3-TEG. This is due to the high efficiency of QW material compared to the Bi_2Te_3 material .

5.3.2 Optimum Coolant Mass Flow Rate

The optimum coolant mass flow rate increased proportional to the vehicle speed and at any given vehicle speed the optimal coolant mass flow rate is lower or approximately equal for the QW-TEG as compared to the Bi_2Te_3-TEG. The exhaust mass flow rate and exhaust inlet temperature increases proportional to the vehicle speed resulting in an increase of the exhaust energy proportional to the vehicle speed. A fraction of this energy was converted to the TEG power and the remainder was rejected to the coolant, resulting in the increase of energy rejected to the coolant proportional to the vehicle speed. Therefore, to lower the rise in cold junction temperature, the optimal coolant flow increased proportional to the vehicle speed. Likewise, a comparison of ZT between the QW and Bi_2Te_3 shows that the efficiency of QW-TEG is higher than the Bi_2Te_3-TEG. Therefore, the QW-TEG generated more TEG power and a

lower quantity of exhaust energy is rejected to the coolant compared to the Bi_2Te_3-TEG, consequently at a given vehicle speed the optimal coolant mass flow rate for the Bi_2Te_3-TEG is higher than the QW-TEG.

5.3.3 Optimum Leg Aspect Ratio

A comparison of the optimum leg aspect ratio between different vehicle speeds using either of the QW or Bi_2Te_3-TEG shows that the leg aspect ratio decreases with increasing vehicle speed. The exhaust inlet temperature and exhaust mass flow rate increases proportional to the vehicle speed and therefore the exhaust heat transfer coefficient increases. As a result, the combined thermal resistance of the heat exchangers decreases. As discussed previously to maximize the TEG power the thermal resistance of the thermoelectric device must match the combined thermal resistance of the heat exchangers. Therefore, the optimum leg aspect ratio decreases with vehicle speed.

In the preceding discussion the design variables are optimized for each vehicle speed. This would not be feasible in an actual device. Therefore, the effect of a single optimum design on the net power is assessed. Using the 50 (mph) QW-TEG optimum design at 30 and 70 (mph) vehicle speeds, the reduction in net power is about 43 and 32.6 % respectively. Thus, a single point design does not perform well over the range of conditions.

An alternative design procedure would be as follows. The exhaust inlet temperature and exhaust mass flow rate at 30 (mph) vehicle speed is a fractional constituent of the exhaust inlet temperature and exhaust mass flow rate at 50 and 70 (mph) vehicle speeds. Therefore the approach would be to design a TEG system with multiple sections, with each section optimized for a range of temperatures and depending on the quantity of exhaust mass flow rate, the exhaust can be channeled

either through a single section or multiple sections. Such a design approach has already been attempted by Crane and Bell [42] and was shown to maximize the performance of the TEG at all the vehicle speeds.

5.4 Effect of System Size on Non-Mobile Applications

In non-mobile applications, there are neither weight penalties nor space constraints, therefore in this section we examine optimum designs when these constraints are removed. In the configuration without the spatial and weight constraints there was no maximum net power with respect to the A_{xy}. The net power increased proportional to the A_{xy} and started to plateau at A_{xy}=10 (m^2). This is shown in the figure (5.12), where a comparison of net power and net power density as a function of A_{xy} are shown.

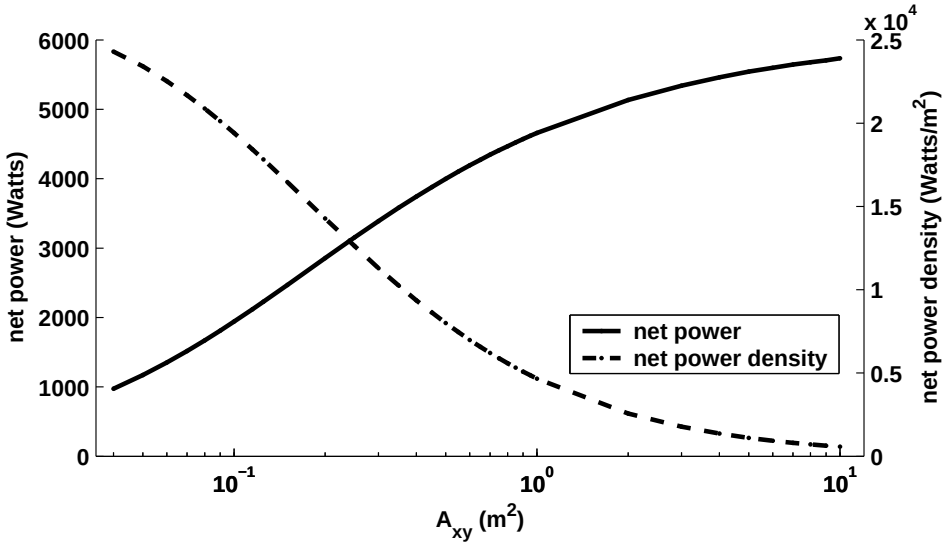

Figure 5.12: Variation of net power and net power density as a function of A_{xy} without the spatial and weight constraints

For stationary applications, economics must be considered to determine the realistic

optimum designs. However, to asses the change in net power and the optimum design with and without the spatial and weight constraints, the results of the configuration without the weight penalty at A_{xy}=0.8 (m^2) are listed in table (5.3).

Table 5.3: Effect of spatial and weight constraints on net power, system size, and optimum design

configuration	net power $(Watts)$	TEG power at shaft $(Watts)$	A_{xy} or opt A_{xy} (m^2)	$\frac{L_x}{L_y}$ or opt $\frac{L_x}{L_y}$	opt $\dot{m}_f$ $\left(\frac{kg}{s}\right)$	opt γ $\left(\frac{1}{m}\right)$
spatial and weight constraints	2994	4056	0.8	1.25	1.5	3.08×10^4
without spatial and weight constraints	4468	4814	0.8	14.7	1.1	2.62×10^4

From the results listed in the table (5.3), without the weight penalty the change in net power is about 50 %. This significant change in net power is due to the change in $\frac{L_x}{L_y}$ ratio and the lack of weight parasitic loss. As discussed previously at a fixed A_{xy} the increase in $\frac{L_x}{L_y}$ ratio increases the exhaust mass flow rate per unit are and consequently the heat transfer and the TEG power. Also, without the spatial and weight constraints the net power and the TEG power increased despite the decrease in optimum coolant mass flow rate. This is due to the fact that the change in (TEG power-blow down work) with respect to the $\frac{L_x}{L_y}$ is significantly greater than the change in (TEG power- coolant pumping power) with respect to the coolant mass flow rate.

Also, the optimum leg aspect ratio without the spatial and weight constraint is lower than with the spatial constraint. As discussed previously, at a fixed A_{xy} the exhaust heat transfer coefficient increases proportional to the $\frac{L_x}{L_y}$ ratio, resulting in the decrease of the combined thermal resistance of the heat exchangers. Therefore,

to maximize the TEG power the thermal resistance of the thermoelectric device must decrease. As the couple density and the system size are fixed, from equation (2.7), the optimum leg aspect ratio decreases proportional to the $\frac{L_x}{L_y}$ ratio to attain a lower thermal resistance of the thermoelectric device.

To summarize, optimization studies were performed to study the effect of system size, flow conditions, thermoelectric material on the net power and the optimum design. To conclude, both the A_{xy} and $\frac{L_x}{L_y}$ ratio had a significant effect on the net power. However, in mobile applications the higher A_{xy} and the higher $\frac{L_x}{L_y}$ is limited by the weight parasitic loss and the spatial constraints. The optimum A_{xy} at which the maximum net power occurs is determined by the competing effects of TEG power and weight parasitic loss and at a fixed A_{xy} the optimum $\frac{L_x}{L_y}$ ratio at which the maximum net power occurs is determined by the competing effects of TEG power and blow down work. The optimum coolant mass flow rate is determined by the competing effects of TEG power and the coolant pumping power. The optimum leg aspect ratio is determined by the competing effects of thermoelectric device power factor and the temperature gradient across the thermoelectric device. The variation of leg aspect ratio is governed by the flow conditions and the thermal resistance matching of the heat exchangers to that of the thermoelectric device. Both the vehicle speed and the thermoelectric material had a significant effect on the net power. However, relatively the effect of vehicle speed is quite significant compared to switching from the Bi_2Te_3 material to the QW material.

Chapter 6

Conclusions and Future Work

In this work a generic TEG simulator was developed. The simulator was used to optimize and determine the optimal TEG system design for a given set of heat exchanger deigns and flow conditions. Two set of thermoelectric materials, QW and Bi_2Te_3, were studied.

The initial optimization studies had shown that there exists multiple optimum designs. Therefore, a study of the response surfaces of the model to variations of the design variables was performed to to ensure that the solution space is fairly smooth without any local minima and the solution is unique. Of the several state space studies that have been performed, it has been found that the combination of couple density and thermoelectric leg aspect ratio resulted in multiple optimum designs. It has been observed that for a given heat exchanger designs, flow conditions, and thermoelectric material, the couple density and leg aspect ratio do not matter individually and only their ratio determines the maximum net and TEG power. Furthermore, at the optimum ratio of couple density to the leg aspect ratio the combined thermal resistance of the exhaust and coolant heat exchangers is equal to the thermal resistance of the thermoelectric device. As a result, the optimization

problem was redefined and the optimization studies have been performed at a fixed couple density.

The optimization studies were performed on a sports-utility vehicle to determine the effect of system size, flow conditions, thermoelectric material on the net power and the optimum coolant mass flow rate and the leg aspect ratio. A few of the primary conclusions are as follows. The A_{xy} and $\frac{L_x}{L_y}$ ratio had a significant effect on the net power. However, in mobile applications the higher A_{xy} and the higher $\frac{L_x}{L_y}$ is limited by the weight parasitic loss and the spatial constraints. The optimum coolant mass flow rate is governed by the competing effects of TEG power and the coolant pumping power and the optimum leg aspect ratio is governed by the competing effects of thermoelectric device power factor and the thermoelectric device thermal conductance.

6.1 Future Work

In this work a TEG simulator was developed and a preliminary set of optimization studies were performed on a mobile application. As discussed in the previous chapters, several of the TEG system design aspects have been included into the simulator and as well as the design optimization itself. However, further refinements to the TEG simulator and additional design optimization studies are necessary to further maximize the TEG power while minimizing the system size. In the following, such design ideas to broaden the current work are introduced and briefly described.

In the state space studies it was established that the maximum TEG power is independent of the couple density and leg aspect ratio and instead can be attained as long as the ratio of couple density to leg aspect ratio is maintained at the optimum. Furthermore, the optimum ratio of couple density to leg aspect ratio is a function of

the flow conditions or rather the exhaust and coolant heat transfer coefficients. In a typical TEG system design, the exhaust and coolant heat transfer coefficients vary along the length of the heat exchangers parallel to the flow. In this work, the couple density was a fixed quantity and the leg aspect ratio was optimized for the complete TEG system. In such a system design approach, the optimum leg aspect ratio will be based on the average flow conditions of the system. Instead, an alternative design approach would be to fix the leg aspect ration based material and manufacturing constraints and optimize the couple density based on the varying flow conditions along the length of the TEG system. Such a system will consist of multiple optimum couple densities along the length of the heat exchangers. Such a design will also maximize the TEG power compared to the approach used in the current work.

All the parametric and optimization studies in this work were performed with a fixed heat exchanger design. An important design variable that might significantly effect the system sizing is the height of the channels in both the EHX and CHX. Therefore, studies must be performed to investigate this particular aspect of the system design.

In the description of the TEG system simulator, it was described that the properties of the thermoelectric legs are estimated by averaging of the properties between the hot and cold junction temperatures. Although, this approach in most cases is a good approximation technique, in some cases accounting for variation of temperature along the leg length and the variation of thermoelectric properties as a function of temperature is required to precisely estimate the thermoelectric device properties [43]. A numerical procedure to account for the variation of temperature along the leg length is developed by Sherman et. al. Therefore, this should be implemented to further increase the accuracy of the current TEG simulator.

In this work, it was assumed that all the thermoelectric couples in the TEG system

are connected in series electrically. Work should be performed to study the effect of various parallel-series configurations on the performance and optimum system design.

Bibliography

[1] D. M. Rowe. Thermoelectrics Handbook. CRC Press, 2006. 1, 6

[2] Aaron Brooker, et al. ADVISOR Documentation. National Renewable Energy Laboratory. 2002. 4, 76

[3] Richard H. Bauer. Auxiliary Electric Power for an Autombile Through the Utilization of a Thermoelctric Generator: A Critical Examination. M of ME Thesis, Department of Mechanical Engineering, Clarkson College of Technology. 1963. 10

[4] Anthony Joseph Tomarchio. A Feasibility Study of Replacing an Electrical Generator of a Standard American Automobile with a Thermoelectric Generator. M of ME Thesis, Department of Mechanical Engineering, Clarkson College of Technology. 1964. 11

[5] Ulrich Birkholz, Erwin Groß, Ulrich Stöhrer, and Karsten Voss. Conversion of Waste Exhaust Heat in Automobile Using FeSi2 Thermoelements. Proc. 7th International Conference on Thermoelectric Energy Conversion. Arlington, USA. 1988. 11

[6] John C. Bass, Norbert B. Elsner, and Ralph Slone. Design Study and Experience with Thermoelectric Generators for Diesel Engines. Proc. Automotive Technology Development Contractors Coordination Meeting. Dearborn, USA. 1990. 11

[7] J. C. Bass, N. B. Elsner, and F. A. Leavitt. Performance of the 1kW Thermoelectric Generator. Proc. American Institute of Physiscs Conference, 1995. 12

[8] Ikoma, K., et al. Thermoelectric Module and Generator for Gasoline Engine Vehicle. Proc. 17th International Conference on Thermoelectrics. Nagoya, Japan, 1998. 12

[9] Douglas Crane, Greg Jackson, and David Holloway. Towards Optimization of Automotive Waste Heat Recovery Using Thermoelectrics. SAE 2001 World Congress, Detroit, MI. March, 2001. 13

[10] J. Vazquez, M. A. Sanz-Bobi, R. Palacios, and A. Arenas. State of the Art Thermoelectric Generators Based on Heat Recovered from the Exhaust Gases of Automobiles. Proceedings of the 7th European Workshhop on Thermoelectrics, Paper:17. Pamplona, Spain. October, 2002. 13, 43

[11] E. F. Thacher, B. T. Helenbrook, M. A. Karri, C. J. Richter. Testing of an Automobile Exhaust Thermoelectric Generator in a Light Truck. Proc. IMechE, Part D: Journal of Automobile Engineering, 221(D1), pp. 95 - 107, 2007. 14, 24, 37, 38, 42, 43, 47, 51, 52, 76, 77

[12] Douglas T. Crane and Gregory S. Jackson. Optimization of Cross Flow Heat Exchangers for Thermoelectric Waste Heat Recovery. Energy Conversion and Management, 45, pp. 1565 - 1582, 2004. 15

[13] Terry J. Hendricks and Jason T. Lustbader. Advanced Thermoelectric Power System Investigations for Light-Duty and Heavy Duty Applications: Part I. National Renewable Energy Laboratory. 15, 16

[14] Terry J. Hendricks and Jason T. Lustbader. Advanced Thermoelectric Power System Investigations for Light-Duty and Heavy Duty Applications: Part II. National Renewable Energy Laboratory. 15, 16

[15] Stanley W. Angrist. Direct Energy Conversion. Allyn and Bacon Inc., 1971. 18, 19, 21, 29

[16] Heikes, R. R. and Ure, R. W. Thermoelectricity: Science and Engineering, Interscience Publishers, New York, 1961. 21

[17] Hi-Z Technology, Inc. <http://hi-z.com/> 2010 (accessed 2010). 24

[18] Madhav A. Karri. Modeling of an Automotive Exhaust Thermoelectric Generator. M of ME Thesis, Department of Mechanical and Aeronautical Engineering, Clarkson University. 2005.

[19] Ghamaty, S. Quantum Well Thermoelectrics for Converting Waste Heat to Electricity, Quarterly Technical Progress Report 9-1-2003 through 12-31-2003, DOE award DE-FC26-03NT41974, Hi-Z Technology, Inc., San Diego, California, January, 2004. 31

[20] Kusch, A. Hi-Z Technology, Inc., personal communication, 2005. 31

[21] Moran, M. J. and Shapiro, H. N. Fundamentals of Engineering Thermodynamics, Fifth Edition. John Wiley & Sons Inc., 2006. 34, 46

[22] Wilke, C. R. A Viscosity Equation for Gas Mixtures, *The Journal of Chemical Physics*, Volume 18, Number 4, April, 1950. 34

[23] Prestone Antifreeze Coolant Properties, Prestone, personal communication, 2003. 34

[24] Kays, M. W. and London, A. L. Compact Heat Exchangers, Reprint Edition (Third). Krieger Publishing company, 1998. xiv, 35, 38, 39, 40

[25] Incropera, F. P. and DeWitt, D. P. Introduction to Heat Transfer, Fourth Edition. John Wiley & Sons Inc., 2002. 36

[26] Karri, M. A., Thacher, E. F., and Helenbrook, B. T. Exhaust energy conversion by thermoelectric generator: two case studies, *Energy Conversion and Management*, in press, 2010. 37, 38, 47, 49

[27] Manglik, R. M. and Bergles, A. E. Heat transfer and pressure drop correlations for the rectangular offset strip fin compact heat exchanger, *Experimental Thermal and Fluid Science*, Volume 10, pp. 171-180, 1995. 37

[28] Lee, P-S., Garimella, S. V., and Liu, D. Investigation of heat transfer in rectangular microchannels, *International Journal of Heat and Mass Transfer*, Volume 48, pp. 1688-1704, 2005.

[29] Kostic, M. and Hartnett, J. P. Heat transfer to water flowing turbulently through a rectangular duct with asymmetric heating, *International Journal of Heat and Mass Transfer*, Volume 29, Issue 8, pp. 1283-1291, 1986.

[30] Jones Jr., O. C. An improvement in the calculation of turbulent friction in rectangular ducts, *Journal of Fluids Engineering*, Volume 98, Series 1, No. 2, pp. 173-181, 1976.

[31] Gnielinski, V. New equations for heat and mass transfer in turbulent pipe and channel flow, *International Chemical Engineering*. Volume 16, pp. 359-368, 1976.

[32] Cornish, R. J. Flow in a pipe of rectangular cross section, *Proceedings of the Royal Society*, 120(A), pp. 691-700, 1928.

[33] Schiller, L. Über den Strönumgswiderstand von Rohrenverschiedenen Querschnitts and Rauhigkeitsgrades, *Zeitschrift fur Angewandte Mathematik und Mechanik*, 3, pp. 2-13,1923

[34] Richter, C. J. Delphi Corporation, personal communication, January, 2004. 47

[35] Graham, C. General Motors Corporation, personal communication, 2002. 47

[36] John Deere, Power Tech 6068H Diesel Engine for Generator Set Applications Specifications, <`http://www.deere.com/en_US/rg/ESC/SpecSheet/GenSet/6068HF475_E_S0_R0.pdf`> , 2010 (accessed 2010). 45, 63

[37] Frank M. White. Fluid Mechanics, McGraw-Hill Inc., New York, 1986. 49

[38] HZ-20 Thermoelectric Module, Hi-Z Technology, Inc. <`http://hi-z.com/hz20.php`> 2010 (accessed 2010). 60, 72, 77

[39] Matlab Documentation. The MathWorks, Inc. 2010. 61

[40] Henderson, J. Analysis of a Heat Exchanger-Thermoelectric Generator System. Proceedings of the 14th Intersociety Energy Conversion Engineering Conference, Boston, MA. pp. 1835-1840, 1979. 72

[41] Stevens, J. W. Optimal Design of Small ΔT Thermoelectric Generation Systems. Energy Conversion and Management, Volume 42, pp. 709-720, 2001. 72

[42] Crane, D. T. and Bell, L. E. Design to Maximize Performance of a Thermoelectric Power Generator With a DynamicThermal Power Source. Journal of Energy Resources Technology, Volume 131, 2009. 92

[43] Sherman, B., Heikes, R. R., Ure, R. W. Calculation of Efficiency of Thermoelectric Devices. Journal of Applied Physics, Volume 31, 1960. 97